Materials Futures

TOPICAL REVIEW • OPEN ACCESS

Recent development of chemically complex metallic glasses: from accelerated compositional design, additive manufacturing to novel applications

To cite this article: J Y Zhang *et al* 2022 *Mater. Futures* **1** 012001

OPEN ACCESS
IOP Publishing | Songshan Lake Materials Laboratory
Materials Futures
Mater. Futures 1 (2022) 012001 (23pp)
https://doi.org/10.1088/2752-5724/ac4558

Topical Review

Recent development of chemically complex metallic glasses: from accelerated compositional design, additive manufacturing to novel applications

J Y Zhang[1], Z Q Zhou[1], Z B Zhang[1], M H Park[1], Q Yu[1], Z Li[2], J Ma[2], A D Wang[3], H G Huang[4], M Song[5], B S Guo[1,6], Q Wang[7] and Y Yang[1,8,9,*]

[1] Department of Mechanical Engineering, College of Engineering, City University of Hong Kong, Kowloon Tong, Kowloon, Hong Kong, People's Republic of China
[2] Shenzhen Key Laboratory of High Performance Nontraditional Manufacturing, College of Mechatronics and Control Engineering, Shenzhen University, Shenzhen, Guangdong 518060, People's Republic of China
[3] School of Materials Science and Engineering, Dongguan University of Technology, Dongguan, Guangdong 523808, People's Republic of China
[4] Institute of Materials, China Academy of Engineering Physics, Jiangyou, Sichuan 621907, People's Republic of China
[5] State Key Laboratory of Powder Metallurgy, Central South University, Changsha, Hunan 410083, People's Republic of China
[6] Institute of Advanced Wear & Corrosion Resistant and Functional Materials, Jinan University, Guangzhou, Guangdong 510632, People's Republic of China
[7] Institute of Materials, Laboratory for Microstructures, Shanghai University, Shanghai 200444, People's Republic of China
[8] Department of Materials Science and Engineering, College of Engineering, City University of Hong Kong, Kowloon Tong, Kowloon, Hong Kong, People's Republic of China
[9] Department of Advanced Design and System Engineering, College of Engineering, City University of Hong Kong, Kowloon Tong, Kowloon, Hong Kong, People's Republic of China

E-mail: yonyang@cityu.edu.hk

Received 1 November 2021, revised 11 December 2021
Accepted for publication 21 December 2021
Published 14 February 2022

Abstract

Metallic glasses (MGs) or amorphous alloys are an important engineering material that has a history of research of about 80–90 years. While different fast cooling methods were developed for multi-component MGs between 1960s and 1980s, 1990s witnessed a surge of research

* Author to whom any correspondence should be addressed.

interest in the development of bulk metallic glasses (BGMs). Since then, one central theme of research in the metallic-glass community has been compositional design that aims to search for MGs with a better glass forming ability, a larger size and/or more interesting properties, which can hence meet the demands from more important applications. In this review article, we focus on the recent development of chemically complex MGs, such as high entropy MGs, with new tools that were not available or mature yet until recently, such as the state-of-the-art additive manufacturing technologies, high throughput materials design techniques and the methods for big data analyses (e.g. machine learning and artificial intelligence). We also discuss the recent use of MGs in a variety of novel and important applications, from personal healthcare, electric energy transfer to nuclear energy that plays a pivotal role in the battle against global warming.

Keywords: metallic glasses, amorphous alloys, alloy design, additive manufacturing, machine learning, high throughput materials design

(Some figures may appear in colour only in the online journal)

1. Introduction

Metals and alloys have been one of the key materials in shaping human society since ancient times. Over the past centuries, human civilization has relied on the discovery and development of new metallic materials which can spur innovation and drive the technologic developments in almost all industrial sectors, from civil and commercial products, high-tech manufacturing to national defense. In light of this, the discovery of the first amorphous alloy by Kramer [1] through electrodeposition in the 1930s marked a new epoch for the research and application of metallic materials. Following Kramer [1], Brenner *et al* [2] produced amorphous Ni–P thin films by electrodeposition in the 1950s. In the 1960s, Duwez *et al* [3] successfully obtained Au–Si glassy ribbons with a thickness of $\sim$10 μm through vacuum melt spinning. With the development of rapid cooling techniques, thicker and larger amorphous metals or metallic glasses (MGs) with more complicated chemical compositions were developed [4–6]. For instance, Chen fabricated Pd-based MGs in a cylindrical shape with a diameter of 3 mm by water quenching in fused quartz capillary in 1974 [5] and after that, Turnbull *et al* obtained a fully glassy ingot with a size larger than 10 mm using the 'boron oxide fluxing' method in 1984 [6]. The 1990s witnessed a surge of research interest in the development of bulk metallic glasses (BMGs), as inspired by the seminar works from Inoue's group in 1990 [7, 8] and from Johnson's group in 1993 [9], both of which successfully obtained a series of BMGs with a diameter ranging from 1 to 15 mm [7–9] through compositional design. These early efforts were even 'translated' into several empirical rules [10–12] in order to guide the development of BMGs with a good glass-forming ability (GFA). Aside from transition metal-based BMGs, Wang's group has developed a series of rare earth metal-based BMGs [13] since 2003, such as La- [14], Ce- [15], and Pr-based [16] BMGs. Today, after almost six decades of intense research, over 800 BMG compositions have been developed and reported in the literature [17], out of which the most studied base elements are Fe, Zr, Ni, Al, Co, Mg, Cu, La, Pd, etc [17], and their percentages are shown in figure 1. To accelerate the compositional search of BMGs, people also utilized novel high throughput methods, such as multi-target physical vapor deposition (MT-PVD) [18, 19] and machine learning (ML) reinforced compositional design [20], to pinpoint the chemical composition with a good GFA. The central theme of research for these efforts has been to make larger and more affordable BMGs with better properties (such as GFA), which however still remains a challenge today.

Apart from the development of BMGs through compositional design, various additive manufacturing (AM) techniques were explored to fabricate bulk structures out of MGs even with poor GFA, which include spark plasma sintering (SPS) [21, 22], selected laser melting (SLM) enabled three-dimensional (3D) printing [23, 24], friction welding [25, 26], electron-beam welding [27, 28], laser welding [29, 30], ultrasound welding, etc [31–34]. The earliest attempt to fabricate bulk sized MGs with AM might be traced back to 1988 when Kawamura *et al* [35] prepared BMGs from ribbons by high temperature sintering. Later in 1994, Kawamura *et al* further adopted warm extrusion to produce Al- [36] and Zr-based [37] amorphous compacts nearly without porosity. In 1999, Inoue's group started to fabricate Fe-based soft magnetic BMGs with SPS [21, 22]. Considering that SPS possesses a very short processing time with better temperature control compared to other powder consolidation methods, people also fabricated Zr- [38], Ti- [39], and Ni-based [40] BMGs successfully through SPS in the first decade of this century. Meanwhile, Sun *et al* [41] attempted to print Zr-based BMGs through laser engineered net shaping in 2008. However, this early effort failed to produce fully amorphous structures because of significant crystallization in heat affected zones. In 2013, Pauly *et al* successfully printed out Fe-based BMGs with a fully amorphous structure and complex shape via SLM [23]. According to reference [24], the cooling rate in the typical heat affected zone can reach as high as 10^6 K s^{-1} in SLM. Notably, many good MG-formers can afford this cooling rate without crystallization, which unlocks the door for SLM enabled 3D printing of BMGs. On the other hand, various welding or joining

Future perspectives
Metallic glasses are well known for their potential engineering applications; however, their widespread use is yet to emerge due to several limitations they are facing, such as the issue of poor glass forming ability and limited size. In this focused review, we discuss the research efforts in tackling this important issue with the tools that were available only recently, such as combinatorial alloy design, big data analysis, machine learning and additive manufacturing. With these novel tools, the design for good performing glass-forming alloys has been greatly accelerated, and bulk structures can be even made of poor glass-forming alloys through additive manufacturing, thereby overcoming the longstanding issue of limited size for metallic glasses. In addition, despite all the limitations facing metallic glasses as a structural material, we also highlight some of their recent applications in biomedical, nuclear and electronic engineering. These progresses deliver a strong message that metallic glasses are still a very attractive material with a bright future ahead.

techniques were developed and studied for the fabrication of BMGs. Since 2001, Kawamura *et al* have studied a number of welding techniques for the fabrication of BMGs, such as electron-beam welding [27], laser welding [29], and explosive welding [31]. In 2014, Jan Schroers *et al* [33] demonstrated the joining of Zr-based BMGs through thermoplastic compression in air. Regardless of the physical mechanisms underpinning these welding methods, they all require that the temperature in the welding area be above the glass transition temperature or melting temperature [33]. More interestingly, Ma *et al* [34] developed a cold joining technique to join MG ribbons or BMGs even at temperatures close to room temperature in 2019. These signs of progress are promising, which suggests that, with these new AM techniques, we may be very close to overcoming the size limit imposed on MGs by the high cooling rate.

To date, there are still several major roadblocks against the widespread structural applications of BMGs, such as medium temperature embrittlement [42], high materials cost, and sustainability [43]; however, their functional applications are attractive and burgeoning. For example, Fe-based amorphous ribbons have already been widely used in China to replace crystalline Fe–Si (silicon steel) in making the next generation electric transformers for their low cost and excellent soft magnetic properties, such as the very low coercivity and high electrical resistance, which can reduce the energy core loss by 70%∼80% [44]. Also, MGs are a good candidate material for the next generation of micro- and nano-devices because of their excellent thermo-plastic formability [39]. Meanwhile, Ti-, Mg- and Zr-based BMGs could be good aerospace and biomedical materials for their high strength, low moduli, and excellent corrosion resistance [45–47]. More importantly, some BMGs were proven to be good catalytic materials, which can be utilized in various applications related to chemical catalysis, such as wastewater degradation [48], water splitting [49], and CO_2 reduction [50]. In this article, we would like to provide a focused overview of the recent advancement in the research of MGs in three fast-growing areas: (a) accelerated compositional design, (b) AM, and (c) new applications.

2. Compositional design of BMG

2.1. Traditional design approach

The traditional design of BMGs has been mainly guided by empirical rules [10, 11, 51, 52], such as the famous Inoue's rules [11], including (a) an atomic size mismatch greater than 12%, (b) highly negative heat of mixing between dislike atoms, and (c) more than three constituent elements. Up to date, the majority of BMGs were discovered and developed based on these rules [10, 11, 51, 52]. However, prior to the proposal of Inoue [11], it was proposed, as early as 1969, that the formation of MGs be correlated with the eutectic or near-eutectic composition of an alloy [51], at which the thermal stability of a metallic liquid can be enhanced, therefore leading to a better GFA. Since then, as guided by this 'eutectic point' rule, a number of BMGs have also been discovered, such as $Zr_{48}Cu_{45}Al_7$ [53, 54], $Zr_{45}Cu_{49}Al_6$ [54], $Zr_{54}Cu_{38}Al_8$ [54], and $Cu_{52}Zr_{40}Ti_8$ [55]. The 'confusion' principle is another empirical rule that is expected to apply to all kinds of BMGs [10], which is also consistent with Inoue's rules [11]. This principle is rooted in the idea that the compositional complexity of an alloy may lead to competitive crystallization of multiple species, thereby causing the 'confusion' (or interruption) of crystallization and facilitating amorphization [10]. At the fundamental level, the confusion principle rule is in line with the theory of Tanaka [52], according to which amorphization is essentially a result of interrupted crystallization because of the strong competition of multiple crystallization processes. Through transmission electron microscopy studies, Wang *et al* [56] found that the excellent GFA of the famous Zr-based BMG (Vitrelloy 1) could be attributed to the confusion principle or the competition between the formation of quasi-crystalline phases and conventional crystals. Over the past six decades, the traditional design approach has been proven useful and successful; nonetheless, by following this traditional design approach, it also means that one usually has to go through iterations of experimental trial and error, which is time consuming, costly and of a low efficiency, particularly when the chemical composition of an alloy becomes complicated, such as high entropy metallic glasses (HEMGs) [57–63] that contain more than five elements mixed in nearly equal molar fractions.

2.2. Combinatorial design approach

To accelerate the compositional design for BMGs, the combinatorial methods have recently attracted a great deal of research attentions [18, 19, 64–70]. These methods are usually based upon high throughput materials synthesis combined with high throughput structure and property characterization. Through the combinatorial design approach, one could prepare and characterize hundreds or even thousands of alloy compositions in a single run of experiment, which greatly improves the efficiency in compositional screening. To date, the most widely used high throughput method for materials synthesis is the MT-PVD [18, 19, 64–66]. In MT-PVD, one can control

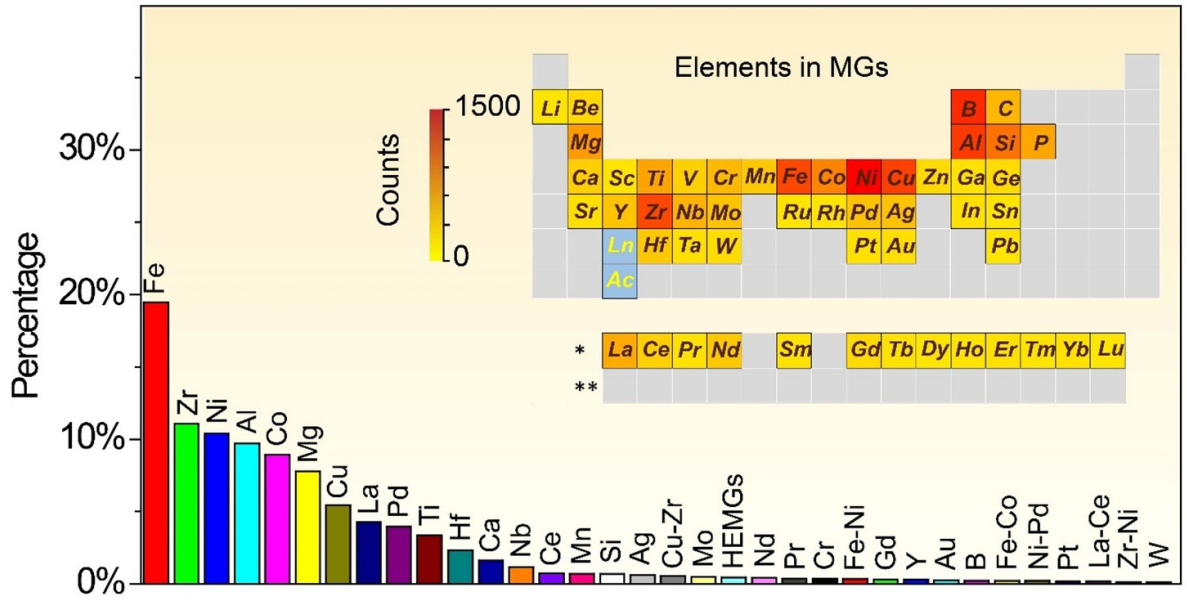

Figure 1. Comparison of different classes of BMGs in terms of their percentage. Note that the comparison is based on a collection of ∼1000 BMGs with measured GFAs. The inset highlights the elements with counts indicating the total number of times an individual element being found in the reported MG compositions. Reproduced from [17]. CC BY 4.0.

the film composition gradient by tuning the angles and intensity ratio among energy fluxes of different targets. Following MT-PVD, rapid x-ray diffraction mapping could be applied to characterize the structure of the metallic thin films as a function of their chemical composition [18, 19, 66], which can quickly lead to the construction of a phase diagram. Aside from x-ray diffraction mapping, people devised other high throughput characterization techniques, such as density mapping [64], electric conductivity mapping [19], and solidification temperature mapping [65]. For example, Li *et al* systematically studied the GFA of the Cu–Zr films through density mapping [64]; Li *et al* searched the high GFA compositions in Ir–Ni–Ta films through electric resistance mapping [19]; and Ding *et al* [65] investigated the GFA of the Au–Cu–Si films [65] through an optical method that enabled the detection of melting and solidification of the metallic films, as seen in figure 2. Ding *et al* also studied BMG-forming compositional space through parallel blow forming, which characterized the thermoplastic formability of the Mg–Cu–Y films and casted quantitative insights into their GFAs [18]. Besides, Tsai *et al* demonstrated that the differential interference contrast optical micrographs could be used to detect amorphous phase through surface topography [67, 68].

Although the MT-PVD method is popular as a high throughput method for materials synthesis, it does not involve explicitly the effect of cooling rate on the formation of amorphous structures. By comparison, the conventional wedge casting may be the first high throughput method that enables the study of various cooling rates, usually in the range of $10^1 \sim 10^3$ K s^{-1}, within one experimental run for a targeted composition [69, 70]. Direct laser AM provides another high-throughput technique to tune the heating/cooling rate, in the range from 10^2 to 10^4 K s^{-1}, through the adjustment of laser power [72], which could be coupled with compositional

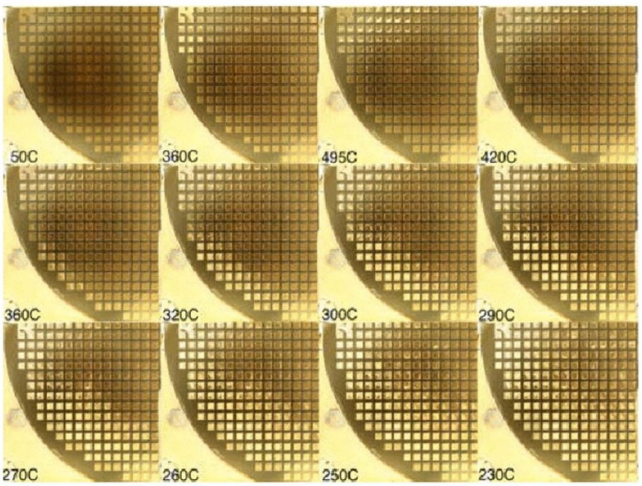

Figure 2. Combinatorial methods for MG synthesis and characterization. The variation of contrast in the heating and cooling cycle of Au–Cu–Si library section. Reprinted from [65], with the permission of AIP Publishing.

mapping to search for the alloy composition with a good GFA [67, 68].

2.3. Data driven design approach

In contrast to the traditional design approach, data driven design approach, such as those based on ML [20, 66, 71, 73–78], provides an alternative to accelerate the compositional design of BMGs. Built upon high-fidelity data, ML has been proven useful, highly efficient in compositional screening for the synthesis of complex materials [20, 79–81]. For the design of next generation BMGs with ML, the sources of high fidelity

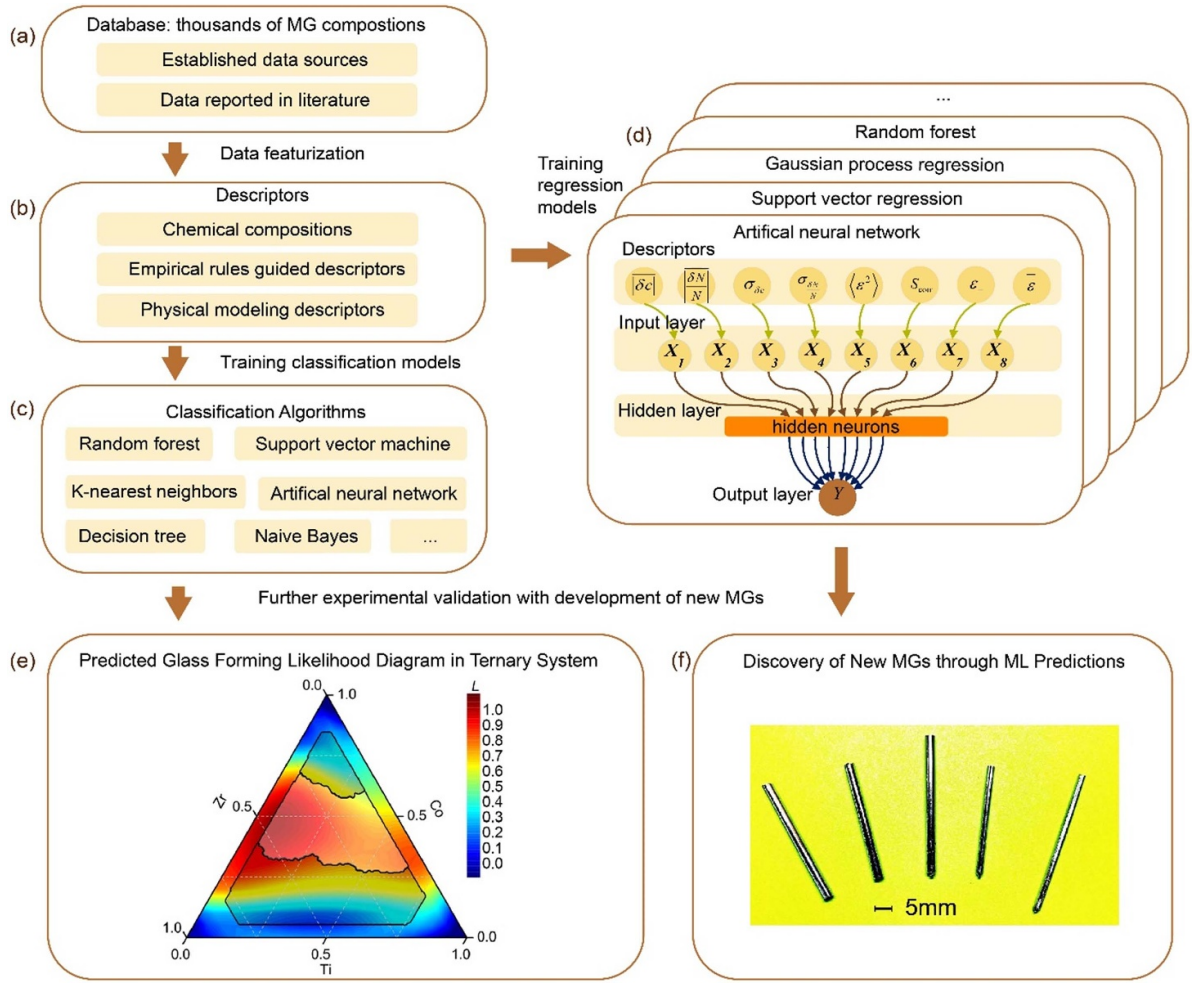

Figure 3. The schematics for developing a machine learning model with classification and/or regression algorithms; (a)–(e) Reprinted from [17]. CC BY 4.0. (a) The MG database with thousands of compositions from established data sources or literature. (b) The development of data descriptors. (c) Classification algorithms used in the study of glass-forming likelihood. (d) Regression algorithms for the prediction of GFA. (e) Contour maps of predicted glass-forming likelihood diagram based on the prediction results of classification model; (f) The development of MGs with high GFA through the prediction of regression model. Reprinted from [71], Copyright (2020), with permission from Elsevier.

data are the pre-requisite (see figure 3(a)). To date, there are a number of data sources available in the open literature for the design of BMGs, such as the handbook by Kawazoe *et al* published in 1997 entitled -*phase diagrams and physical properties of nonequilibrium alloys* [82], and the handbook by Kawazoe *et al* published in 1997 entitled—*nonequilibrium phase diagrams of ternary amorphous alloys* [83]. In addition, different authors also built their own database by collecting data from the existing BMG literature, such as the database built by Long *et al* in 2009 [84], by Tripathi *et al* in 2015 [73], by Ward *et al* in 2018 [76], and by Zhou *et al* in 2021 [17]. Unfortunately, since people tended to collect good data (good glass-forming alloys) while discarded bad by tradition, the positive data for good glass-forming alloys significantly outnumbers the negative ones in most of the existing databases, as noted recently by Liu *et al* [71] and Zhou *et al* [17]. To date, it is still an ongoing research effort and challenge to develop reliable ML models for the discovery and development of next generation BMGs considering the inconsistency and round-up errors in the reported GFA data from different groups, and the imbalance between the positive and negative data in the available databases.

With the established dataset, people have applied a variety of ML algorithms to study MGs with a good glass-forming likelihood [17, 71, 74–76, 78, 79, 85–87] (see figures 3(b), (c) and (e)) or a good GFA [17, 74–76, 87–92] (see figures 3(b), (d) and (f)). These mainly include support vector machine (SVM) [17, 74, 78, 79, 92], random forest (RF) [17, 66, 75, 76, 90], Gaussian process regression (GPR) [17, 74] and artificial neural network (ANN) [17, 71, 79, 87, 89]. However, to effectively train an ML model, one has to design proper 'fingerprints' or descriptors for their data (data featurization), as shown in figure 3(b). At the present time, data featurization is mostly based on the chemical composition of alloys [78, 87, 91] or by translating a chemical composition into empirical parameters guided by the aforementioned empirical

Table 1. The up-to-date reported BMG/MG compositions discovered by machine learning.

Composition	Year	Data descriptors	Algorithms	D_{max} (mm)	References
$Zr_{59.2}Cu_{16.2}Ni_{12.6}Al_{9.6}Hf_{2.2}Ti_{0.2}$	2021	8 descriptors based on physical models	Adaptive boosting, GPR, ANN, SVM, RF	5	[17]
$Zr_{65}Cu_{17.5}Ni_{10}Al_{7.5}$	2018	213 descriptors based on empirical rules	RF	4.4	[76]
$Zr_{60}Cu_{17.5}Ni_{10}Al_{7.5}Ti_5$	2018	213 descriptors based on empirical rules	RF	4.2	[76]
$Zr_{55}Cu_{23}Al_{12.5}Ni_{7.5}Ti_2$	2018	213 descriptors based on empirical rules	RF	3.8	[76]
$Zr_{47}Cu_{23.5}Al_{15}Ni_{11.5}Ti_3$	2018	213 descriptors based on empirical rules	RF	3.1	[76]
$Zr_{55}Cu_{20}Al_{15}Co_{10}$	2021	8 descriptors based on physical models	Adaptive boosting, GPR, ANN, SVM, RF	3	[17]
$Zr_{54}Ni_{16}Cu_{14}Ti_{10}Al_6$	2021	8 descriptors based on physical models	Adaptive boosting, GPR, ANN, SVM, RF	3	[17]
$Zr_{55}Cu_{20}Co_{10}Ti_8Al_7$	2021	8 descriptors based on physical models	Adaptive boosting, GPR, ANN, SVM, RF	3	[17]
$Zr_{51}Co_{39}Al_{10}$	2021	52 descriptors based on chemical compositions	Correlation-based neural network	3	[87]
$(Zr_{62}Co_{32}Al_6)_{95}Si_5$	2021	52 descriptors based on chemical compositions	Correlation-based neural network	3	[87]
$(Zr_{63}Co_{24}Al_{13})_{95}Ni_5$	2021	52 descriptors based on chemical compositions	Correlation-based neural network	3	[87]
$Zr_{47}Cu_{23}Ni_{18}Al_{10}Ti_2$	2018	213 descriptors based on empirical rules	RF	2.4	[76]
$Zr_{48}Cu_{29.5}Al_{18}Ni_{4.5}$	2018	213 descriptors based on empirical rules	RF	2.2	[76]
$Zr_{55}Cu_{20}Ti_{10}Co_{10}Al_5$	2021	8 descriptors based on physical models	Adaptive boosting, GPR, ANN, SVM, RF	2	[17]
$Zr_{45}Cu_{20}Ti_{10}Al_{10}Co_{10}Hf_5$	2021	8 descriptors based on physical models	Adaptive boosting, GPR, ANN, SVM, RF	2	[17]
$(Zr_{58}Co_{11}Al_{31})_{95}W_5$	2021	52 descriptors based on chemical compositions	Correlation-based neural network	2	[87]
ZrHfAlCo	2021	8 descriptors based on physical models	Adaptive boosting, GPR, ANN, SVM, RF	0.05	[17]
ZrHfAlCoCu	2021	8 descriptors based on physical models	Adaptive boosting, GPR, ANN, SVM, RF	0.05	[17]
ZrHfAlCoNiCu	2021	8 descriptors based on physical models	Adaptive boosting, GPR, ANN, SVM, RF	0.05	[17]
TiZrHfCo	2021	8 descriptors based on physical models	Adaptive boosting, GPR, ANN, SVM, RF	0.05	[17]
TiZrHfAlCo	2021	8 descriptors based on physical models	Adaptive boosting, GPR, ANN, SVM, RF	0.05	[17]
TiZrHfAlCoCu	2021	8 descriptors based on physical models	Adaptive boosting, GPR, ANN, SVM, RF	0.05	[17]

rules [66, 71, 74–76, 88–90, 92], such as mean atomic size [74, 75, 79, 87], atomic size difference [71, 74, 79, 90], mean atomic volume [74, 90], mixing enthalpy [74, 75, 79, 87], ideal mixing entropy [71, 74, 75, 79, 87], mean electronegativity [75, 79, 87, 90], electronegativity difference [71, 79], valence electron concentration [71, 75, 79, 87] and calculated density [71, 75, 87]. If one considers all individual and collective attributes of constituent elements, the number of the data descriptors designed based on the empirical rules could reach 186 [76], which suggests the intrinsic complexity of the ML based design of BMGs. However, according to Ghiringhelli [93] and Zhang *et al* [94], this high dimensionality of data descriptors is not conducive to effective data mining, which can easily cause problems such as overfitting and high calculation cost. Through physical modeling guided ML, Zhou *et al* recently developed ML models with only 8 data descriptors [17]. Despite the challenges above mentioned, people have discovered a number of new glass-forming alloys, some of which can be cast in bulk forms (see table 1 for details).

3. Additive Manufacturing (AM)

3.1. AM based on hot fusion

3.1.1. AM based on supercooled liquids. In parallel to compositional design, AM has also been considered as an alternative approach to fabricate BMGs by joining MG feedstock in the form of powders, debris, or cut pieces [22, 95]. Considering the poor workability and inhomogeneous plastic flow of MGs below T_g [96], the AM techniques based on liquid state fusion (or hot fusion) have been developed and long utilized for achieving strong metallurgical bonding between MGs [29, 32, 35]. In principle, liquid state fusion of MGs can be achieved in the following two ways. First, one could join MGs by increasing the working temperature to a value between the glass transition temperature, T_g, and the onset crystallization temperature, T_x [96]. In this temperature range, also termed as supercooled liquid region (SCLR), metallic liquids flow in a non-Newtonian fashion [96], enabling long-range diffusion of atoms that leads to the bonding of MGs with the assistance of high pressure [97, 98]. Besides hot fusion in SCLR, AM can be also based on molten liquids. In a molten liquid, atomic diffusivity is significantly enhanced so that no external pressure is needed for hot fusion. In practice, hot fusion based AM of MGs can be achieved through SPS [21, 22, 35, 38–40, 95, 99–104], friction joining/welding [25, 26, 29, 105–109], thermoplastic compression [33, 98, 110, 111] and selective laser melting [23, 24, 48, 112–118].

While sintering or consolidation of solids can be traced back to the early works during 1920∼1950 [102], Kawamura *et al* developed the method of high-temperature sintering to produce BMGs in 1988 [35]. Back then, Kawamura and co-workers ground MGs ribbons about 20 μm thick into powders and were able to sinter these powders in their SCLR into a bulk rod with a diameter of 6 mm and height of 3.5 mm. In addition, Kawamura *et al* also developed other sintering methods for MGs, such as warm extrusion in 1994 [36] and pulsed current sintering in 1999 [21], also termed later as SPS [102]. As illustrated in figure 4(a), in a typical SPS process, MG powders are first filled into a vacuum chamber and are subsequently subject to a pulsed high direct current and pressure. During sintering, a local electrical breakdown can take place between powders, generating plasma to clean adsorbed gases and to break refractory oxide films [21]. As a result, the hot fusion of MGs in their SCLR through SPS can achieve nearly full densification within a short period of time and under low pressures [22, 35, 95, 102]. To date, SPS is still one of the most suitable and popular manufacturing trajectories for viscous or hot fusion of MG powders [100]. In order to achieve high densification in SPS, a greater pressure (normally $\leqslant$500 MPa), longer holding duration, and a higher loading temperature are usually required [22, 38, 40], which however needs more expensive tooling (e.g. SiC or WC) [100, 103] and can also facilitate crystallization in MGs [39, 104]. While optimization of SPS for various MGs is still an open issue, people have successfully fabricated a variety of BMGs through SPS, as shown in figure 4(b), including Fe-based [22], Cu-based [104], Al-based [99], Mg-based [101], Ni-based [40], Ti-based [39], and Zr-based BMGs [38].

Different from SPS, friction welding, as patented in the 1890s [119], is able to join bulk samples of different shapes via a rotary, linear or orbital mode [120]. In 2001, Kawamura *et al* joined $Pd_{40}Ni_{40}P_{20}$ rods by rotary friction welding [25]. As illustrated in figure 4(c), in a typical rotatory friction welding process, one workpiece is rotated around its central axis (left) while the other keeps stationary but in alignment with the rotating one (right). The friction heat generated at the interface leads to material softening and extrusion (figure 4(d)) in order to establish strong metallurgical bonding [25, 26, 29, 105, 106]. Through rotary friction welding, people already fabricated MG–MG [105, 107] and MG-crystalline composites [26] with a strong and tough welding interface [26, 105, 107]. Recently, friction stir welding [108] and friction stir spot welding [109] were also developed to join MGs.

On the other hand, while the viscous flow of MGs in their SCLR has long been considered as an avenue for thermoplastic forming and net-shape processing [121, 122], Kuo *et al* successfully adapted thermoplasticity to join BMGs in vacuum in 2010 [98]. Later, Schroers *et al* demonstrated that thermoplasticity can even join BMGs in air subject to a pressure that is sufficient to crush brittle native oxides [33], as illustrated in figures 4(e) and (f). In such a case, once two fresh BMGs are brought to contact, thermoplasticity enabled joining can take place within milliseconds or seconds [33]. In this way, people fabricated BMG honeycomb-like architectures [110]. To date, optimization of the thermoplasticity enabled joining is still a topic of active research [111]. Apart from the above-mentioned methods, we note that the joining of BMGs in their SCLR can be also realized via reactive foil welding [123] and small-scale resistance spot welding [124].

3.1.2. AM based on molten liquids. Aside from SCLR, AM can be also carried out by heating MGs above their melting temperatures. As atomic diffusion is greatly enhanced in this temperature range, which enables metallurgic bonding even without external pressure, the challenge becomes how one can avoid crystallization in the fusion zone and/or the heat-affected zone during cooling [30, 32, 33]. In the 2000s, Kawamura *et al* successfully weld BMGs by heating up their temperatures into the range of molten liquids through electron-beam welding [27, 28, 126], spark welding (pulse-current welding) [32], and explosive welding [31, 127, 128]. In these early attempts, the welding time was kept short, merely 10^{-2}∼10^{1} s [29, 32] and some of the weldments appeared as hard as their master alloys [27, 28, 32]. However, these early methods could merely fabricate crystal-free weldments among a few good glass formers, such as Zr- and Ti-based BMGs [27, 28, 31, 32, 126–130], which had a critical size larger than 10 mm. According to Shen *et al* [129], the cooling rates in these methods were estimated to be around 10^3 K s^{-1}, which may not be sufficient for joining marginal glass formers without crystallization.

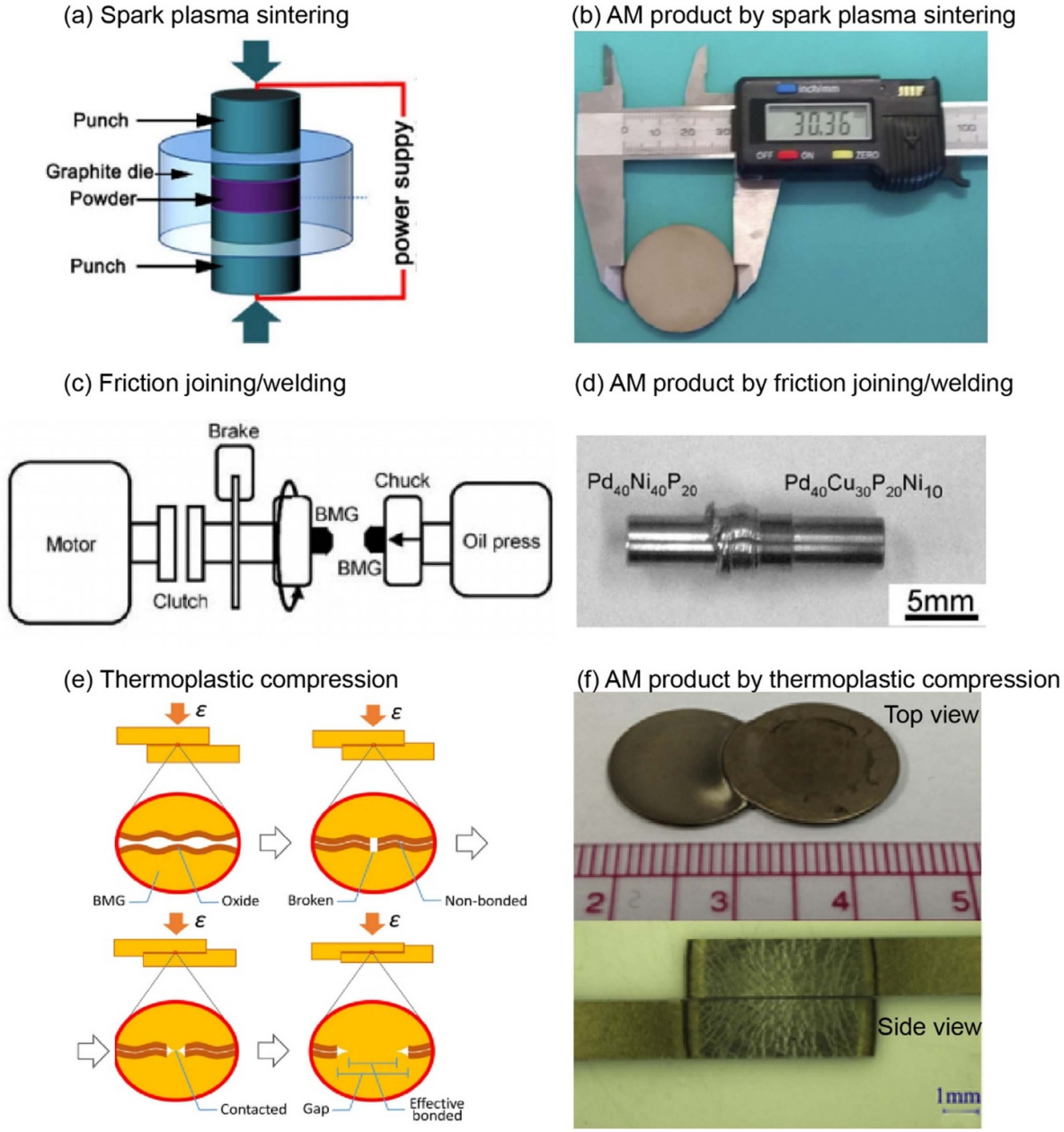

Figure 4. The schematic diagrams for the AM techniques based on supercooled liquids and the photo of a typical AMed BMG sample. (a) and (b) spark plasma sintering (SPS); (a) was reprinted from [125]. CC BY 4.0. (b) Reprinted from [100], Copyright (2016), with permission from Elsevier; (c) and (d) friction joining/welding; (c) Reprinted from [29], Copyright (2004) with permission from Elsevier; (d) Reprinted from [105], Copyright (2004) with permission from Elsevier; (e) and (f) thermoplastic compression; (e) Reprinted from [111], Copyright (2020), with permission from Elsevier; (f) Reprinted from [33], Copyright (2003), with permission from Elsevier.

By comparison, laser melting is considered more suitable to join BMGs in their molten liquid state [30], owing to its high energy density, narrow spot size, and deep weld penetration [131]. In 2006, Li *et al* successfully laser-welded two pieces of $Zr_{45}Cu_{48}Al_7$ BMGs without causing crystallization at the cooling rate well above 10^3 K s^{-1}, as calculated by finite element simulations [30]. Subsequently, in order to further improve the quality of laser welding, people upgraded the laser sources by employing those with a higher power [132], a deeper penetration (e.g. fiber laser) [133], and a shorter welding duration (e.g. pulsed laser) [134, 135]. With the updated lasers, weldments could attain almost the same tensile strength as the corresponding base alloys [135, 136]. Despite these successful applications of laser welding, laser-BMG interactions, which involve heating, cooling, and crystallization, in a typical laser welding process are not fully understood from a theoretic viewpoint [131, 135], which to a certain degree hinders the wide use of laser welding.

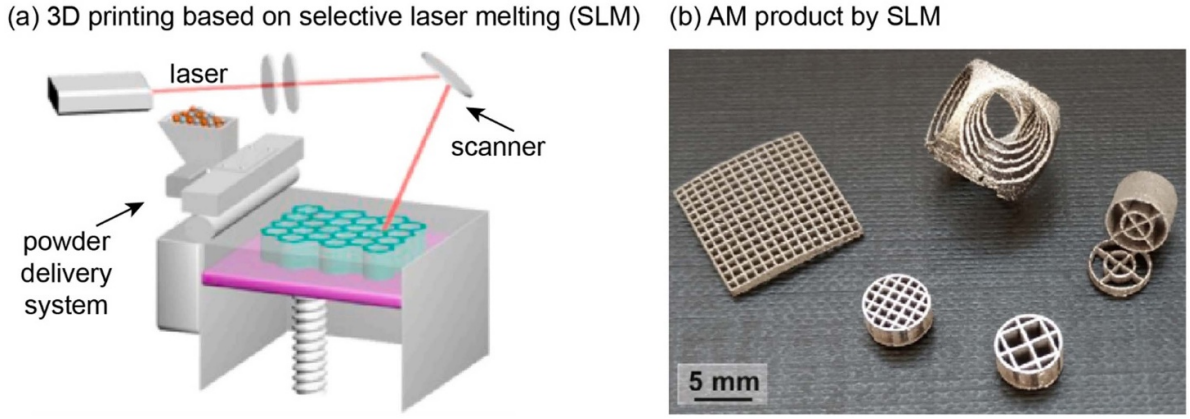

Figure 5. (a) The schematic diagram and (b) the photo of printed BMG structures with selective laser melting (SLM). Figure (a) Reprinted from [24], Copyright (2021), with permission from Elsevier; (b) Reprinted from [112], Copyright (2017), with permission from Elsevier.

Apart from laser welding, laser based 3D printing is another attractive AM technique to produce BMGs. According to the recent review article by Zhang *et al* [24], the up-to-date laser based 3D printing techniques to fabricate BMGs include selective laser melting (SLM), laser engineered net shaping, thermal spray 3D printing, laser foil 3D printing, fused filament fabrication, and laser forward transfer 3D printing. Among these 3D printing techniques, SLM may be the most popular method to be reported from 2013 to 2021 [137]. By comparison, SLM enables a high cooling rate ($10^4 \sim 10^6$ K s^{-1}) [23, 138], a better dimensional precision with a laser spot of $10^2 \sim 10^3$ μm [137, 139], and good control of geometric complexities [112]. Figure 5(a) sketches one typical operational mechanism of SLM, for which thin layers of MG powders are paved onto a base plate subject to the scanning melting of a laser beam guided by the galvano mirrors (scanner) in order to build a 3D structure layer by layer (figure 5(b)). At the current moment, the main issues with SLM-ed BMGs are to reduce their porosity while increasing their volume fraction of amorphous structures. To address these issues, people proposed three strategies which are related to laser energy densities, laser scanning trajectory, and MG powders, in order to improve the quality of 3D printed BMGs [24, 112–114, 140]. In comparison to cast bulk alloys, 3D printed BMGs are generally less stiff (lower elastic modulus), softer (lower strength), and less ductile [24] owing to the presence of micro-pores [140] and the precipitation of brittle intermetallic [48, 115, 116]. While these defects (pores and precipitates) are detrimental to the general structural applications, they are conducive to the functional applications of SML-end BMGs [48], such as for catalysis [117] and bioimplants [118].

3.2. AM based on cold fusion

Recently, a fast cold fusion technology has been proposed for MGs based on high-frequency ultrasonic vibration processing, namely ultrasonic AM, which can bypass the defects generally induced by thermal effects, such as crystallization, oxidation, and element segregation [141]. As shown in figure 6(a), the ultrasonic vibration loading with a frequency of 20 kHz is applied on the single kind of MG ribbons or mixed MG ribbons, and then the dense bulk MG with metallurgical bonding can be rapidly obtained within 1 s [34]. It should be noted that the joining temperature of MGs during the ultrasonic AM is much lower than T_g, indicating that a new bonding mechanism dominates the cold fusion rather than anchoring or adhesion in SCLR [142]. The surface activation analysis of MGs by dynamic scanning probe microscopy shows that the mobility of the atoms on the surface is significantly influenced by the activation frequency, as shown in figure 6(b), the viscoelastic loss tangent (tanδ) correlating with internal friction almost increases to four times as the driven frequency shifting from 200 Hz to 70 kHz, this high tanδ value under ambient temperature is close to that of bulk samples near T_g. Meanwhile, the corresponding surface viscosity decreases to three orders of magnitude as the activation frequency increases to 70 kHz. These results demonstrate that the high-frequency vibration significantly improves the surface atom mobility, and thus enhancing the atomic diffusion in the bonding interface, which enables the fast cold fusion of various MG ribbons to synthesize composites with metallurgical interfaces among different alloy systems, such as Pd–Zr, Pd–La and Pd–Zr–La MG systems (figures 6(c) and (d)). In addition, by utilizing this reliable bonding behavior, the composites of MGs and other materials can also be fabricated by ultrasonic AM [143]. As shown in figure 6(e), the Zr-based MG ribbons mixed with high entropy alloy (HEA) ribbons are subjected to the ultrasonic loading for several seconds, then the bulk composite sample with a tunable proportion of rigid amorphous phase and soft crystalline phase can be facilely achieved (figure 6(f)). This design strategy produces an exceptional toughening effect due to the synergic deformation mechanisms of shear bands and dislocations.

Theoretically, the dynamic evolution of amorphous atomic structure under ultrasonic vibration can be described by a phenomenological model consisting of densely packed clusters (elastic matrix) and loosely packed clusters (liquid-like units) in MGs [144, 145]. Those liquid-like units can largely absorb

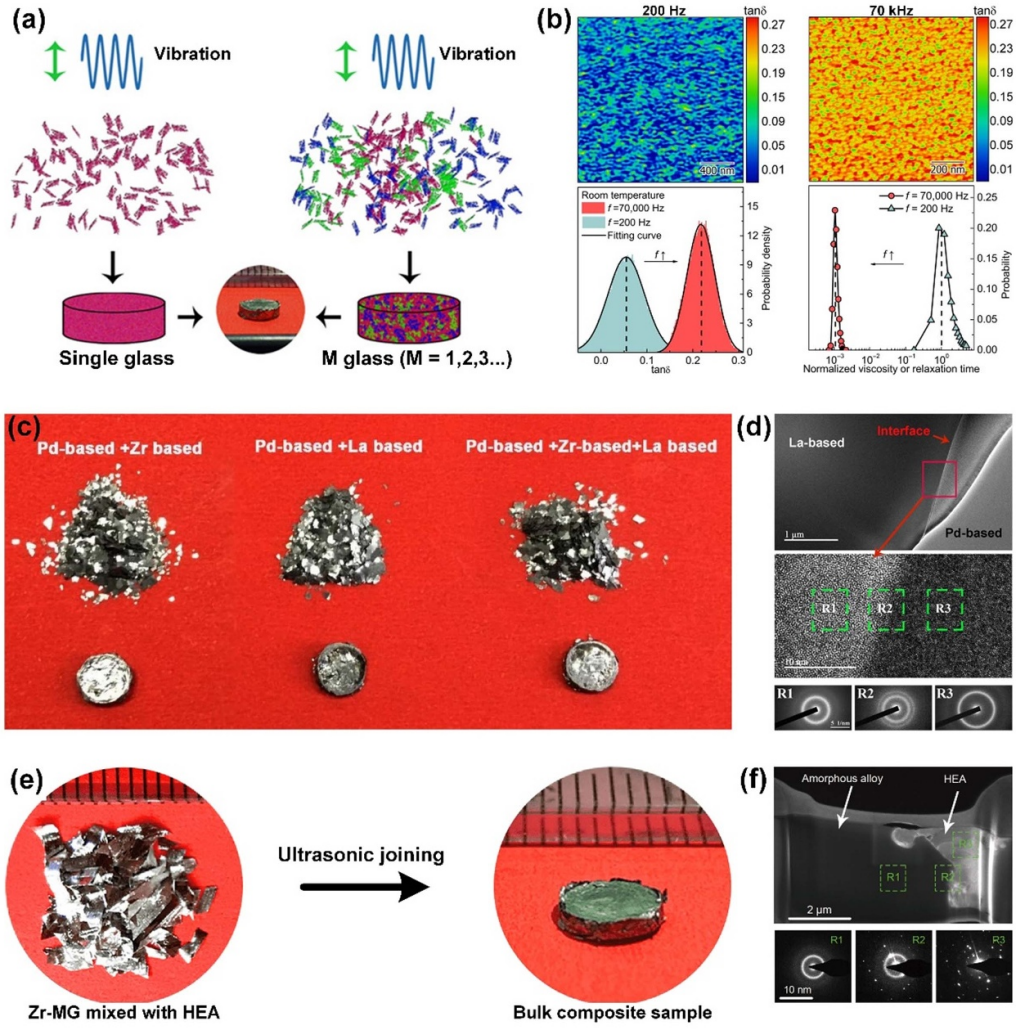

Figure 6. (a) The schematic diagram to fabricate single- and multi-phase bulk sample by ultrasonic cold joining of the MG ribbons, (b) The MG interfaces activation and bonding mechanism under ultrasonic vibration, (c) Bulk composite sample of Zr-MG and HEA synthesized by ultrasonic joining, (d) The micro-sectional morphology of the HEA/MG composite, and the corresponding TEM diffraction images at different positions, (e) The shear bands formed in the MG matrix in the fracture surface of the composite under compression loading, (f) The strong embedding effect of HEA particles in the MG matrix observed in the fracture surface, (g) Stress-strain curve of HEA/MG composite obtained by ultrasonic additive manufacturing, comparing to that of the single HEA and MG, (a)–(g) adapted from [143] (2020) (© 2022 Springer Nature Switzerland AG. Part of Springer Nature.). With permission of Springer.

the high-frequency vibration energy and enhance the mobility of the atoms due to the nature of viscoelasticity and low stiffness, which can loosen the densely packed clusters and extend the liquid-like regions. This variation of the amorphous structure will induce significantly softening behavior and viscous flow of MGs [146–149]. Based on this mechanism, the ultrasonic AM process can be applied to the fast cold fusion of BMGs at a very low pressure. Thus far, various pairs of BMGs including Pt–Pt, Pt–La, La–La, Pd–Pd, and Zr–Zr have been successfully bonded by ultrasonic vibration, under short processing time (<1 s) and low loading (<1 MPa) (figures 7(a) and (b)). Most importantly, the interface temperature captured by infrared thermal imaging during the ultrasonic joining is far below the T_g of the selected MGs [150, 151]. The high-resolution CT detection and SEM observation confirm the metallurgical bonding of BMGs (figures 7(c)–(e)), and the bonding interface retains the amorphous atomic arrangement (figures 7(f) and (g)). The molecular dynamics simulation demonstrated that the surface atoms require less energy to pass through the damaged oxide layer and diffuse to another side than that of the bulk interior (figure 7(h)). Thus the interface atom diffusion can be significantly accelerated to realize rapid bonding at an ambient temperature. Besides, the high instantaneous strain induced by ultrasonic loading can effectively break the rigid oxidation layer that acts as a barrier for forming reliable bonding between interfaces. And the subsequent viscous flow of MGs under ultrasonic vibration is also beneficial to the removal of oxidation debris, producing pristine MG surfaces for metallurgical bonding. The ultrasound assisted cold fusion strategy provides a new solution for the rapid AM of MGs and synthesizes novel MG matrix composites with tunable functions.

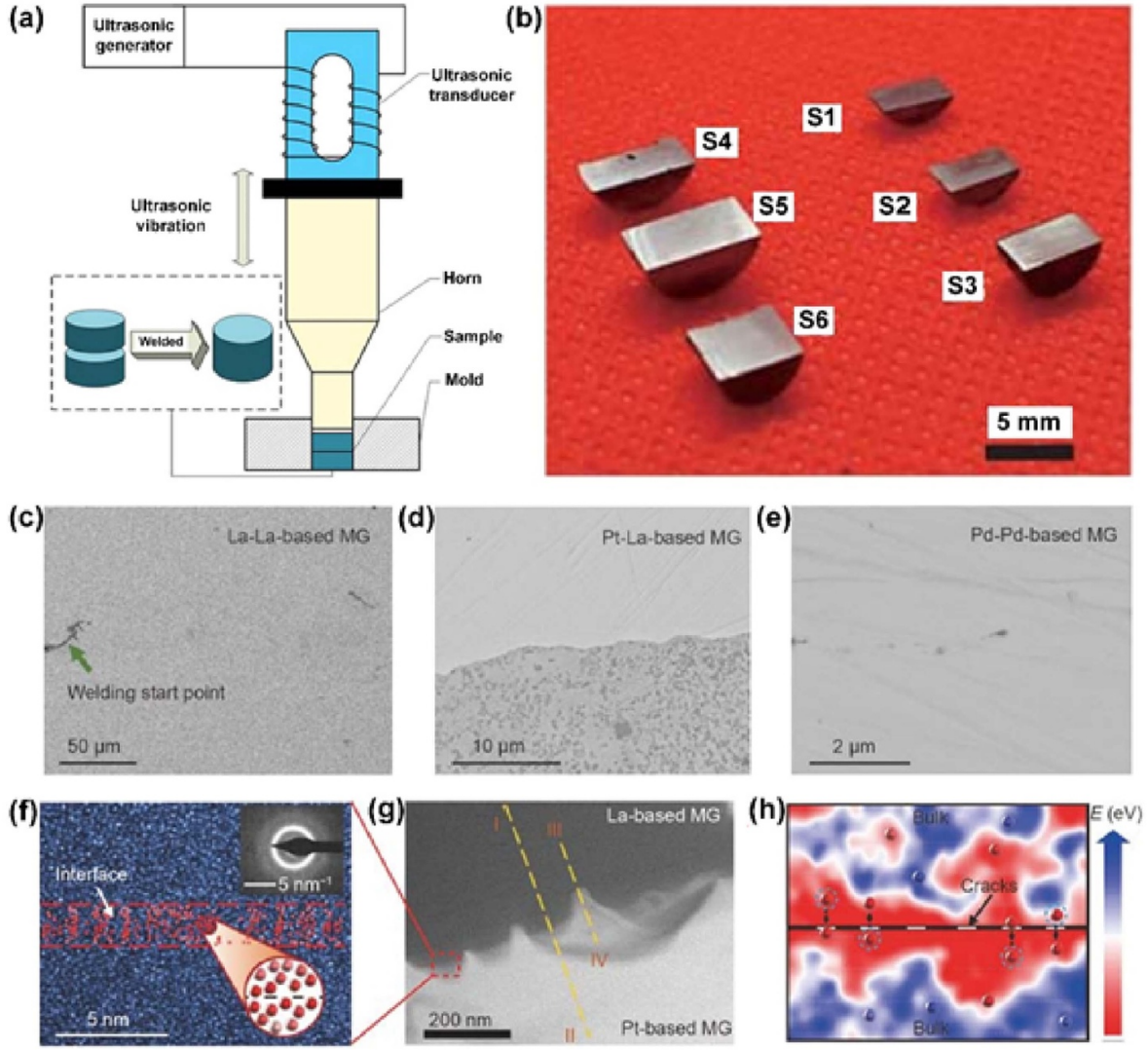

Figure 7. (a) The schematic diagram of ultrasonic joining of BMGs; Reprinted from [150], Copyright (2020), with permission from Elsevier. (b) Various pairs of BMGs bonded by ultrasonic cold fusion; Pt–Pt-based MG (S1), Pt–La-based MG (S2), La–La-based MG (S3), Pd–Pd-based MG (S4), Zr–Zr-based MG1 (S5), and Zr–Zr-based MG2 (S6). (c)–(e) SEM image of bonding interface of La–La-based MG, Pt–La-based MG, and Pd–Pd-based MGs, respectively. (f)–(g) High-resolution TEM and SAED pattern of the bonding interface of Pt–La-based MG obtained by ultrasonic cold fusion. (h) Molecular dynamics simulation of atomic mobility of MGs showing that the activated energy required for the surface atoms is lower than that in the bulk; (b)–(h) Reprinted from [151], Copyright (2021) © 2022 Springer Nature Switzerland AG. Part of Springer Nature.). With permission of Springer.

Now, we would like to discuss the pros and cons of different AM techniques. Although hot fusion based AM techniques (e.g. laser based 3D printing and SPS) have been well established after years of dedicated research, which can be easily integrated into existing production lines for industrial scale mass production [22, 38–40, 99, 101, 104] and were already proven to be applicable to a wide range of MG compositions and geometrically complex shapes [23, 24, 112], the MG bulk structures and/or products so fabricated usually exhibit poor strength, low densification and even undesirable crystallization. By comparison, the cold fusion based AM techniques are just emerging and their applicability to different MG compositions is yet to be confirmed. However, the issue of undesirable crystallization at high temperatures can be mitigated in cold fusion of MG powders or ribbons. Here, we note that the bulk MG structures fabricated through cold fusion can nearly retain the density and strength of their feedstock materials [34], which is promising and warrants further research.

4. Recent applications of chemically complex MGs

4.1. HEMGs for refrigeration

The notion of HEMGs is related to HEAs [57], the latter of which is expected to exhibit a simple solid solution phase because of a high configurational entropy of mixing resulting from the mixing of multiple principal elements. To HEMGs, this so-called high entropy effect is more related to the confusion principle [57], which assumes that viable crystallization could be interrupted because of the competition of multiple

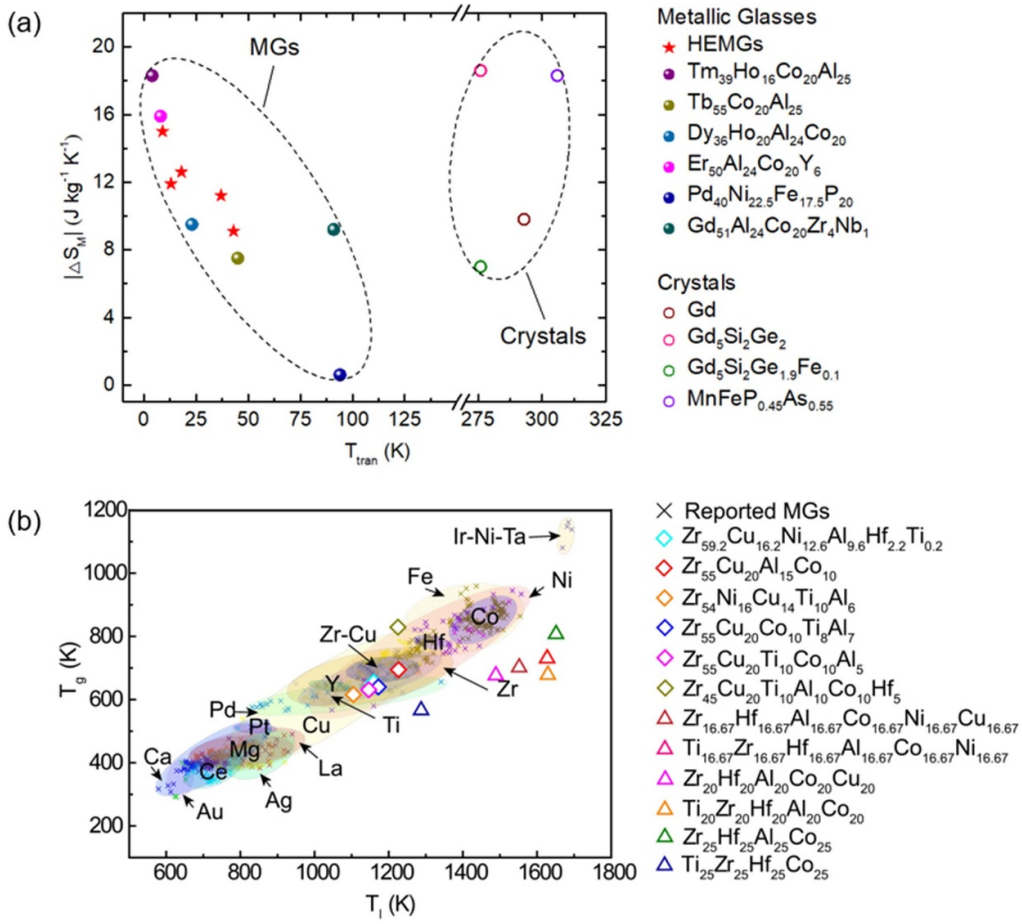

Figure 8. (a) A comparison of the magnetic entropy changes ($|\Delta S_M|$) under 5T and transition temperature (T_{tran}) among MGs and crystalline magnetic refrigerants [158, 159]. (b) Summary of T_g versus liquidus temperature of various MGs; Reproduced from [17]. CC BY 4.0.

crystallization processes in a multi-principal element alloy, hence leading to a stable metallic liquid and ultimately vitrification when supercooled. Compared to conventional MGs, such as Zr- and Fe-based MGs, HEMGs do not have a unique base element and therefore their configurational entropy of mixing is expected to be greater.

Indeed, the first report of HEMGs can be traced back to the early work of Ma *et al* in 2002 [152], two years before the publication of the seminar works about HEAs by Yeh *et al* [153] and by Cantor *et al* [154] in 2004. In this 2002 paper, Ma and co-workers developed a series of Ti–Zr–Hf–Cu–M (M=Fe, Co, Ni) HEMGs [152]. After that, however, the research of HEMGs was seemingly shadowed by that of conventional MGs until a surge of renewed interest was seen in 2011 [59, 62]. Up to date, a variety of HEMGs were discovered with their critical size ranging from micro- to centi-metres [155]. Although the study of HEMGs is still in its infancy, people already discovered some interesting HEMGs, such as the $Ti_{20}Zr_{20}Cu_{20}Ni_{20}Be_{20}$ HEMG [63] with the critical diameter of 3 mm and its variant (by introducing Hf) with the critical diameter of 15 mm [61], the $Sr_{20}Ca_{20}Yb_{20}(Li_{0.55}Mg_{0.45})_{20}Zn_{20}$ HEMG with an extremely low T_g and elastic modulus that can be imprinted even at room temperature [59], and the $Fe_{25}Co_{25}Ni_{25}Mo_5P_{10}B_{10}$ HEMG with a high refrigeration capacity (RC) because of its large magnetic entropy change (ΔS_M) [156]. Here, it may be worth noting that, compared to the prototypical magnetocaloric alloy $Gd_5Si_2Ge_2$ with $|\Delta S_M| = 18.6$ J (kg K)$^{-1}$ and RC = 305 J kg^{-1}, the $Ho_{20}Er_{20}Co_{20}Al_{20}RE_{20}$ (RE = Gd, Dy, and Tm) HEMG reported by Huo *et al* [157] has $|\Delta S_M| = 15.0$ J (kg K)$^{-1}$ and RC = 627 J kg^{-1}, which is twice of that of $Gd_5Si_2Ge_2$. The excellent magnetocaloric effect makes these HEMGs an attractive candidate alloy for magnetic refrigeration. Nonetheless, the GFA of the magnetocaloric HEMGs is poor. Li *et al* [158] replaced Ho in the above HEMG and obtained the magnetocaloric $Er_{20}Dy_{20}Co_{20}Al_{20}RE_{20}$ (RE = Gd, Tb and Tm) HEMGs with an improved GFA. Significantly, we note that the transition temperature (T_{tran}) of these HEMGs is much lower than 100 K, in contrast to $T_{tran} > 273$ K for typical crystalline magnetic refrigerants [159]. This behavior implies a promising application of these HEMGs as a potential refrigerant alloy in the helium and hydrogen liquefaction temperature range (figure 8(a)). Recently, Zhou *et al* [17] developed a series of HEMGs through ML, of which the primary crystalline products show outstanding thermal stability, as shown in figure 8(b). Compared to conventional MGs, the liquidus temperatures (T_l) of these newly developed HEMGs are much

higher than what the empirical rule from conventional MGs suggests $T_l/T_g \sim 2/3$. This high thermal stability of the primary crystalline products in the HEMGs may be attributed to a high entropy effect.

4.2. Uranium-based MGs for nuclear energy

Uranium and its alloys are valuable nuclear fuel materials, but their applications are usually hindered by poor corrosion resistance due to the high chemical activity of uranium. In order to improve their corrosion resistance, amorphization of U alloys by rapid liquid quenching was explored with different means, such as splat quenching, arc-furnace quenching, and vacuum melting spinning, by people in the US in the 1970s, such as Ray *et al* [160], Giessen *et al* [161], and Drehman *et al* [162], who reported glass formation in uranium-TM (transition metals: V, Cr, Mn, Fe, Co, Ni, Pd, Ir, Os) binary systems and U–Cr–V ternary system [163]. However, glass transition could not be easily observed in the calorimetric analysis of these U-based alloys. Notably, the heat release upon crystallization of the U-TM MGs was determined to be in a range of 3∼7 kJ mol^{-1}, which is comparable to those of some ordinary MG formers. Also, people only performed a preliminary evaluation of the corrosion resistance of the $U_{70}Cr_{30}$ and $U_{70}V_{30}$ MGs in 1976 by merely examining if there was any change in their surface color [160].

To tackle the issue of global warming, nuclear energy as a source of clean energy provides a feasible solution to the world. Compared to the conventional ceramic UO_2 fuel, which has a relatively low thermal conductivity and low U content (just ∼33 at. % U), metallic nuclear fuels are more attractive because of their higher thermal conductivity and richer U concentration. In addition, we note that amorphous metallic fuels contain abundant free volumes (e.g. extra volumes between constituent elements), which leads to a stronger fission gas capacity than their crystalline counterparts. Recently, the group led by Huang *et al* [164–179] performed a systematic study of U-based BMGs. By means of multi-component alloying and micro-alloying, they developed a few ternary or pseudo-ternary MG systems, such as U–Co–Al [173, 179], (U, B)–Co–Al [173], U–Fe–Sn [178], and U–Fe–Al [164]. With melt spinning, glassy samples can be prepared in a large compositional range for the U–Co–Al or U–Fe–Al systems [164, 179]. Notably, these newly designed U-based MGs showed $T_g > 600$ K, $T_x > 630$ K, and $T_g/T_l > 0.6$, among which $U_{60}Fe_{27.5}Al_{12.5}$ may be considered as the best glass former with $T_g = 635$ K, ΔT_x ($T_x - T_g$) = 48 K, $T_g/T_l = 0.612$. Apparently, the GFA of $U_{60}Fe_{27.5}Al_{12.5}$ is comparable to that of some Zr-, La-, and Mg-based BMGs [164]. At the fundamental level, crystallization of U-based MGs seemed to be governed mainly by crystal nucleation with the activation energy of 210∼240 kJ mol^{-1} [168, 176]. Here, it is worth mentioning that Al-containing U-based MGs displayed excellent corrosive resistance in neutral solutions as a consequence of the amorphous structure and the formation of a compact aluminum oxide film. To make U-containing BMGs, sphere-dispersed glass matrix composites were successfully synthesized *in-situ* with suction-casting and tilt-casting, as seen in figure 9. These composites can be manufactured for a wide composition range of U (from 3 to 40 at.%) and in a dimension of at least 15 mm in diameter. A typical $U_{30.03}Zr_{28.83}Ti_{9.66}$ $Ni_{7.00}C_{u8.7}5Be_{15.73}$ composite exhibited a compressive fracture strength of 1.7 GPa and high corrosion resistance in both neutral and alkaline media [174].

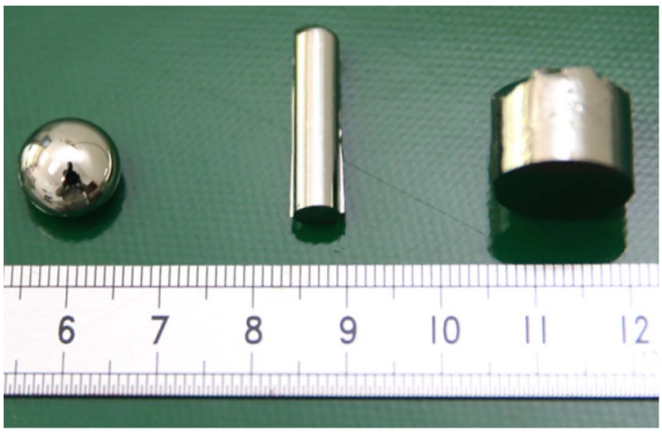

Figure 9. The photograph of U-based glass matrix composites; Reprinted from [174], Copyright (2018), with permission from Elsevier.

Compared to other MGs, U-based MGs commonly display low liquid fragility (m) values of 20∼28, indicating that they are strong glass formers. Furthermore, unlike other MGs, the elastic modulus of the U–Co–Al MGs seemingly does not obey the simple rule of mixture, the latter of which suggests that the elastic properties of MGs should be the weighted average of those of their constituent elements. Such two phenomena are interesting and worth further research, which might be attributed to the electronic structure of U, such as their 5f electrons. In general, these U-based MGs with a high U concentration (>60 at. %) exhibit the merits of high strength, good corrosion, and irradiation resistance, which endows them with great potential as a new fuel material in next generation nuclear fuel reactors. Therefore, we expect that the U-based MGs could play a pivotal role in the battle against global warming and also in helping various countries, such as China, to achieve carbon-neutral development. Besides, the elements making up U-based MGs usually have a large atomic weight difference, which is quite appealing in the fundamental study of MGs, such as the correlation between nano-scale heterogeneity and mesoscale properties.

4.3. Copper based MGs for antibacterial surfaces

Despite the ever-increasing investment in the medical and healthcare field, the threat from hospital-acquired infections (HAI) remains significant. Moreover, the adverse effects of HAI can be further aggravated by the emergence of antibiotic-resistant bacteria. According to predictions in recent reports, the global costs of antibiotic resistance will reach 100 trillion $ and 10 million lives annually in 2050. To tackle such a severe situation, in addition to discovering novel antibiotics, other

supplemental antimicrobial agents are also urgently needed. As an effective approach, antimicrobial metal materials such as copper and silver have been widely used since ancient times to limit microbial activity. In comparison to silver, the high antibacterial effect coupled with its relatively low cost have made copper the preferred material for touch surfaces, and Cu element has already been implemented in some healthcare settings [180]. However, the poor wear resistance of copper limits its long-term applicability, which could be addressed by developing Cu-based BMGs [181], because they can unify the antimicrobial effectiveness of copper and high hardness, excellent wear and corrosion resistance, and smooth surface of BMGs.

In the past decades, researchers have demonstrated that some types of Cu-based BMGs exhibit good antibacterial activity, such as $Cu_{50+X}(Zr_{44}Al_6)_{50-X}$ (X = 0, 3 and 6) [182], $Cu_{48}Zr_{42}Ti_4Al_6$ [183], and $Cu_{(62\sim64)}$–$Hf_{(36\sim38)}$ [181], and their antimicrobial effectiveness depends on the Cu content. For example, González *et al* [182] indicated that the higher Cu content results in a higher reduction in colony-forming units for *Escherichia coli* (gram-negative) and *Bacillus subtilis* (gram-positive) after 60 min of contact time for the Cu–Zr–Al BMGs. The improvement of antimicrobial effectiveness was ascribed to the higher concentration of Cu ions released from Cu-based BMGs, because the Cu ions can eliminate bacteria with three possible mechanisms [184, 185]: (a) the interference to the permeability of cell membrane; (b) the degradation of genomic and plasmid DNA, and (c) the generation of reactive hydroxyl radicals through a Fenton-type redox reaction which can cause oxidation of proteins and lipids.

The studies previously described have been mostly focused on optimizing the chemical composition of materials to control their antimicrobial effectiveness. Nevertheless, other factors, including surface morphologies [186] and oxidation [187], crystalline phases content [188] are also at work. For instance, Villapún *et al* [187] demonstrated that the oxidation can increase the antimicrobial performance of the Cu-based BMGs, and the improvement can be explained by the fact that interphase boundaries could constitute the easy diffusion paths for Cu ions release, while the needle-shape structure of oxides could trigger mechanosensitive channels to promote the migration of copper ions into the cell. Furthermore, Villapún *et al* also reported that the surface texture can improve the antimicrobial ability of $Cu_{55}Zr_{40}Al_5$ BMGs. Thus, it is believed that the surface modification can be adopted as an effective post approach to enhance the antimicrobial performance of Cu-based BMGs.

Although the bulk samples are useful as a screening method to investigate the effects of chemical composition and surface structure of Cu-based BMGs for desired antimicrobial performance, once the most promising compositions and surface structure are selected, they have to be produced as coatings in order to exploit their antimicrobial effectiveness in the healthcare sector. Eskandrany *et al* [189] coated the $Cu_{50}Ti_{30}Ni_{20}$ film onto the SUS304 alloy by cold spraying technology and demonstrated that $Cu_{50}Ti_{30}Ni_{20}$ film can remarkably inhibit colony formation of *E. coli* compared with bare SUS304. Based on the above literature review, it can be confirmed that the Cu-based BMGs are promising candidates for antimicrobial application, but the studies on Cu-based BMGs concerning their antimicrobial performance are still in their infancy.

4.4. Iron based MGs for electric transformers

Fe-based MGs have been widely used in electrical and electronic devices, including transformers, motors, etc, owing to their low coercivity (H_c), high permeability (μ_e), and low core loss [190]. Their typical boundary-free and long-range-disordered microstructure results in an ultra-low pinning effect on the magnetic domain and superior soft-magnetic properties [191]. Compared with the commercial Si-steel, the relatively lower B_s limits the wide application of commercial MGs, therefore motivating us to explore new alloy and process design strategies [192–197]. The conventional alloy design concept based on a homogeneous microstructure and high glass formability (GFA) has approached the limit to improve magnetization (B_s) of MGs [194–197] considering the trade-off between GFA and B_s as shown in figure 10(a). From the application viewpoint, the improvement of B_s without the sacrifice of GFA is important for the miniaturization of electric devices with attractive energy-saving and high-efficiency advantages.

Recently, Wang *et al* reported novel alloy design concepts based on the high-entropy, cluster stabilization, and magnetic-intercoupling enhancement mechanisms [194, 198, 199] [shown in figures 10(b) and (c)]. By using these new approaches, $Fe_{82.7–85.7}Si_{2–4.9}B_{9.2–11.2}P_{1.5–2.7}C_{0.8}$ MGs with a distinctly high Fe content of 93.5–95.5 wt.% were readily developed [198] (see figure 10(d)). However, it was subsequently found that the high Fe content does not lead to an expected super-high B_s, and it appears that the maximum B_s is attained when the Fe content reaches about 80%, such as in the $Fe_{84.2}Si_{2.1}B_{11}P_{1.9}C_{0.8}$ alloy [198] as illustrated in figure 10(a). As inspired by these results, Zhao *et al* changed to a new strategy for a stronger magnetic-interaction by incorporating Co/Ni in the high Fe-content alloys and developed $Fe_{71}(Co, Ni)_{15}B_{9.5}Si_2P_2C_{0.5}$ alloys with a high B_s value up to 1.86 T via the fourfold combinational approaches [200]. This strategy should apply to a wide range of Fe-based MGs in overcoming the B_s-GFA trade-off. Moreover, it is worth noting that the high Fe-content alloy ribbon is ductile and can withstand 180° bending prior to fracture, which is desirable for engineering applications as shown in figures 10(e) and (f) [198, 201].

4.5. Refractory MGs for applications under extreme conditions

Over past decades, refractory metallic glasses (RMGs) have attracted increasing attention owing to their great potential for use in many applications, such as military, aerospace, energy production, etc [202–204]. Similar to other types of MGs, RMGs exhibit high strength, high hardness, and high resistance with respect to wear or corrosion [204]. More importantly, RMGs display extremely high thermal stability against

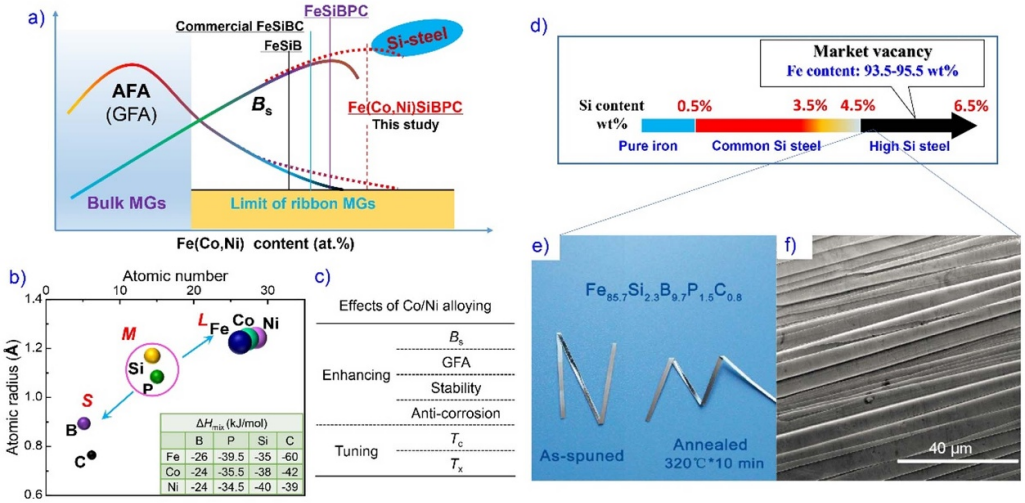

Figure 10. (a) Dependences of GFA and B_s on the ferromagnetic element (Fe(Co, Ni)) content in different alloy systems, showing the GFA and B_s limits in the Fe-based metallic glass. (b) Atomic number and radius of the component elements in Fe(Co, Ni)SiBPC alloys (inset shows the mixing enthalpy). (c) Other influences of Co/Ni alloying; (a)–(c) [200] (2021) © 2022 Springer Nature Switzerland AG. Part of Springer Nature.). With permission of Springer. (d) Fe content of the electric steels and commercial MGs [198]. (e) Image of annealed $Fe_{85.7}Si_{2.3}B_{9.7}P_{1.5}C_{0.8}$ ribbon after bending for 180°. (f) SEM image of the shear zone in the bending region; (d)–(f) [198] (2017) © 2022 Springer Nature Switzerland AG. Part of Springer Nature.). With permission of Springer.

crystallization at high temperatures (>700 °C) [204]. As a result, RMGs could be an ideal candidate material for use in a highly corrosive and high temperature environments, such as in molten salts or supercritical water often used in nuclear power plants [205, 206].

Being one prototypical RMG, iridium-based MGs (e.g. Ir–Ni–Ta–(B)) were developed recently by Li *et al* [19] using combinatorial methods. According to [19], the iridium-based Ir–Ni–Ta–(B) MGs were found to possess a high T_g, T_x, good GFA, and high-temperature strength in addition to high resistance against corrosion and oxidation. According to the recent study [19], the boron-containing Ir–Ni–Ta based MG exhibits a high T_g of 889 °C and a wide SLR of 136 °C, indicative of their superior thermal stability. Moreover, we note that, while the Ir–Ni–Ta MGs can be synthesized into 2 mm-diameter glassy rods in a wide compositional range that contains 20%–35% Ir, 35%–40% Ta, and 25%–40% Ni, the addition of B can significantly enhance its GFA with the critical diameter increased to 3 mm [6]. Also, as the temperature rises near T_g, the Ir–Ni–Ta system exhibits unprecedented strength of >4 GPa, unlike other conventional Ir- and Co-based BMGs that show notable drop in strength. Moreover, similar to other typical high-temperature alloys such as Inconel 718, these Ir–Ni–Ta MGs can retain their high-temperature strength even at high temperatures [19].

Recently, it was reported that the Ir–Ni–Ta MGs had excellent mechanical and chemical properties at micro-/nano-scales. For instance, Wang *et al* [207] reported that Ir–Ni–Ta MGs displayed a large plastic strain up to 35% in micro-compression with the micropillar size ranging from ∼500 nm to ∼5 μm; and its yielding strength can reach up to 7 GPa, remarkably higher than those of most metallic materials. Furthermore, the enhancement of deformability for Ir–Ni–Ta MGs at a small scale has been rationalized in terms of the competition between the cracked-induced fracture instability and the intrinsic shear instability. In light of these results, it was suggested that the Ir–Ni–Ta MGs might be used in next generation micro-devices that are expected to deploy at high temperatures or under extreme conditions [207].

Furthermore, Wang *et al* [208] found that the $Ir_{25}Ni_{33}Ta_{42}$ RMG nanofilm exhibits high intrinsic activity and superior stability at an ultralow Ir loading of 8.14 μg cm^{-2} for hydrogen evolution reaction (HER) in 0.5 m H_2SO_4. The Ir-based RMG film is believed to be the most active HER heterogeneous catalysts in terms of an overpotential of 99 mV for a current density of 10 mA cm^{-2}, a small Tafel slope of 35 mV dec^{-1}, and high turnover frequencies of 1.76 and 19.3 H_2 s^{-1} at 50 and 100 mV overpotentials respectively. When compared to other catalysts, such as MGs, sulfides, phosphides, and precious-metal-containing catalysts (see figure 11), the HER performance of the $Ir_{25}Ni_{33}Ta_{42}$ RMG film is exceptionally good, which may be attributed to a synergistic effect of alloy composition and amorphous structure [208].

4.6. MG coatings for healthcare

Although the structural applications of BMGs are hindered by their low temperature brittleness, low dimensional MGs (e.g. thin films [47], nanowires [209], nanotubes [210], nanomembranes [211]) attracted a great deal of interest in different fields, such as nano-devices [212], microfabrication [213], bio-implants [214], even healthcare [47] and electrocatalysis [215]. Owing to the plasticity size effect [216, 217], low dimensional MGs are generally ductile and stretchable. For instance, compared with conventional metallic and ceramic coatings, MG thin films possess an excellent combination of strength and ductility, as seen in figure 12(a)

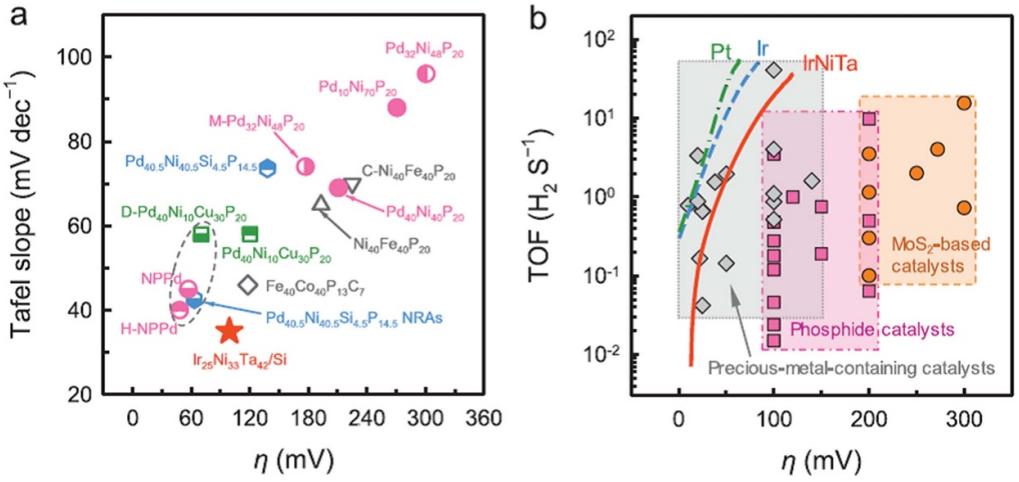

Figure 11. (a) Tafel slope versus the overpotential at 10 mA cm^{-2} for the $Ir_{25}Ni_{33}Ta_{42}$ MG film or HER in 0.5 $_M$ H_2SO_4 and other existing MG catalysts for HER. (b) turnover frequency (TOF) values averaged over all surface sites of the $Ir_{25}Ni_{33}Ta_{42}$ MG film compared with the Ir film, Pt film, and other highly active HER catalysts, including molybdenum sulfide-based catalysts, transition metal phosphides, and precious-metal-containing catalysts; [208] John Wiley & Sons. [© 2019 WILEY-VCH Verlag GmbH & Co. KGaA, Weinheim].

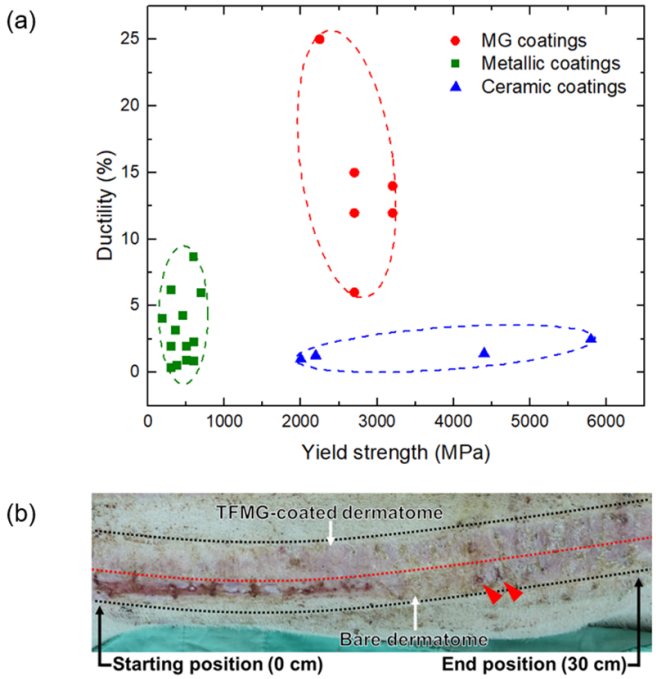

Figure 12. (a) A comparison plot of ductility versus yield strength of various coating materials; Reprinted from [218], Copyright (2020), with permission from Elsevier. (b) The wound healing after seven days for hairless skin grafting; Reprinted from [221], Copyright (2019), with permission from Elsevier.

[218]; therefore, they are considered as an ideal candidate coating material for structural applications. In addition, some metallic-glass thin films, such as $Ti_{50}Cu_{42}Ni_8$, are biocompatible and were already proven to have no cytotoxicity effect on biological cells [45]. By alloying with Cu and Ag, the metallic-glass thin films (e.g. $Zr_{61}Al_{7.5}Ni_{10}Cu_{17.5}Si_4$) even show outstanding antimicrobial capabilities [219]. This unique combination of mechanical and biomedical properties renders metallic-glass thin films with a great potential for applications in the biomedical and healthcare industries.

In 2017, Cai *et al* [214] coated the commercial Ti–6Al–4V, the widely used alloy for dental implant, with the $Zr_{60.14}Cu_{22.31}Fe_{4.85}Al_{9.7}Ag_3$ thin film. As a result, the fretting resistance of the coated dental implant increased by almost 3 times with a decreasing bio-corrosion rate. On the other hand, due to the absence of crystalline microstructures and defects, metallic-glass thin films can attain a much smoother surface than crystalline films, particularly after appropriate annealing [220]. Making use of this attribute, people can improve the smoothness and sharpness of surgical blades by coating them with metallic-glass films. For instance, Chu *et al* [221] coated cutting blades with the $Zr_{53}Cu_{33}Al_9Ta_5$ metallic-glass thin film, which could reduce the cutting force of microtome blades by ∼51%. Meanwhile, the metallic-glass coatings can reduce the increase in the roughness of dermatome blades from 70% to only 8.6% after their use in a split-thickness skin graft surgery for hairless skin. Meanwhile, the wounds left by the MG-coated blades were noticeably smaller, as seen in figure 12(b), which could be attributed to the smoother surface and thus a lower coefficient of friction. Apart from surgical blades, metallic-glass films can be also coated onto medical needles, which are another common tool that needs a low insertion force and hence a less resultant trauma. Up to date, metallic-glass thin films have already been coated on dental needles [222] and tattoo needles [223]. A good example is the 304 stainless-steel dental needles coated with the $Zr_{53}Cu_{33}Al_9Ta_5$ metallic-glass thin film. After coating, the insertion (or retraction) force of a 304 stainless-steel dental needle was reduced by ∼66% (or ∼72%) when the needle was inserted into (or retracted from) a polyurethane rubber block [222]. Notably, this beneficial effect came along with the reduction in the coefficient of friction by one order of magnitude. As tattooing became a fashion recently worldwide, non-sticky tattoo needles, which can retain tattoo patterns while diminishing skin injuries, became

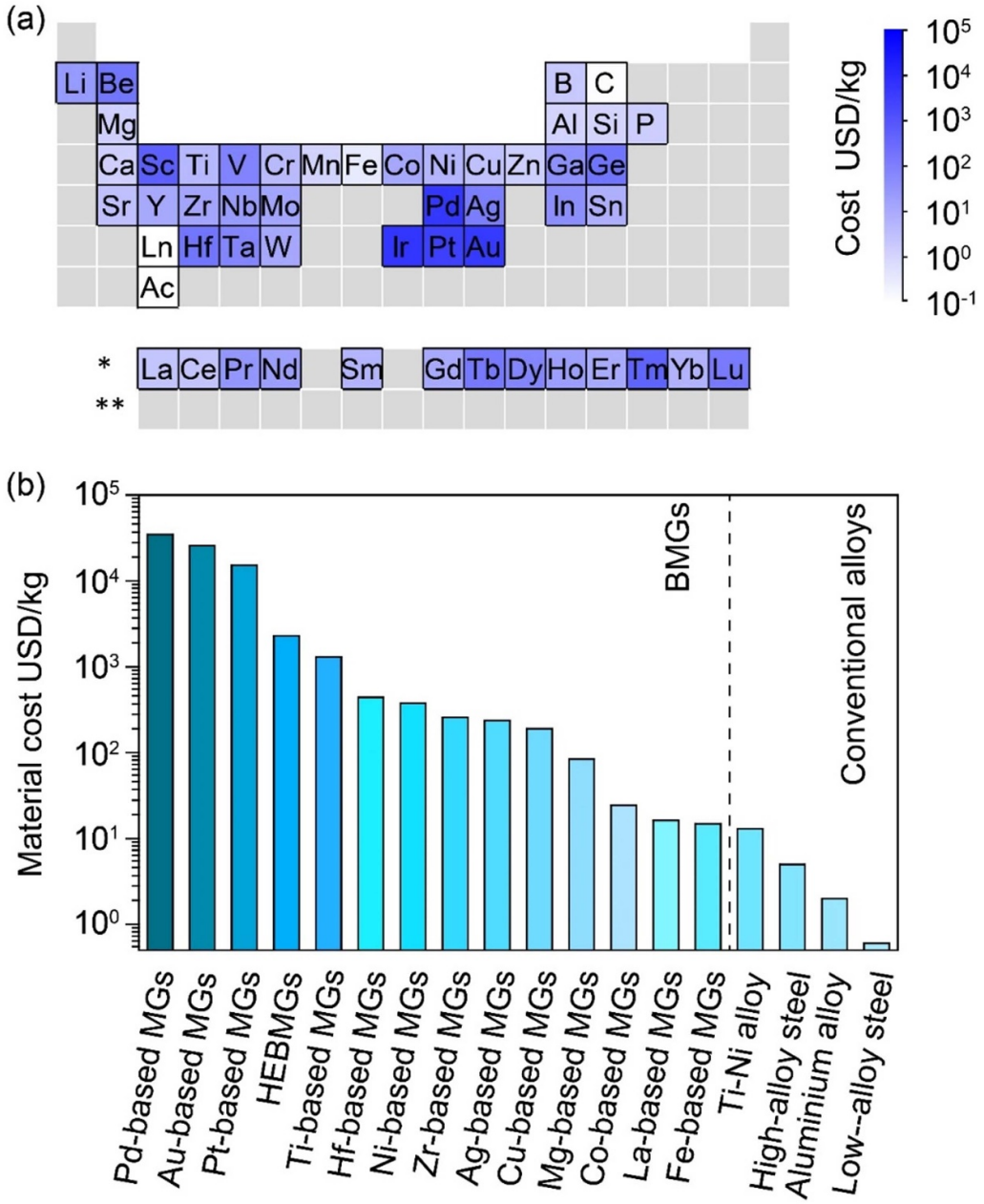

Figure 13. (a) The prices of elements in forming MGs. (b) A material cost comparison between different types of BMGs and conventional alloys.

attractive. Recently, Chu *et al* [223] coated tattoo needles with the $Zr_{62.4}Cu_{22.4}Al_{9.8}Ni_{5.4}$ thin films, which showed less tissue adherence after insertion and improved performance by preventing 57% spread of pigments to surrounding skins. With the MG-coated needles, one can attain very fine tattoo lines and make a high-resolution tattoo pattern. Most importantly, the use of the MG coated needles can lead to the closure of trauma within 2 h after insertion and only five days are needed for entire healing, which is significantly faster than that created by bare needles.

Before moving to the summary, we note that, despite the excellent thermoplastic formability and castability of MGs, most of them contain precious and/or rare-earth metals, such as Pd, Au, Ag, Zr, Hf, Be, and others , as shown in figure 13(a). Therefore, the price of MG-made products could be much higher than those made of conventional alloys. This poses an issue of economic viability for any real applications of MGs. Figure 13(b) compares the estimated material cost of MGs in comparison to that of Ti–Ni alloys, Al alloys and steels. Evidently, the materials cost of MGs could be several orders of magnitude higher than those conventional alloys. Undoubtedly, these extremely high price makes MGs unaffordable or replaceable in conventional applications, particularly considering their low temperature brittleness under tension [42]. In addition, MGs can easily crystallize at temperatures above T_x, which can lead to crystallization induced embrittlement [122]. Therefore, they are not suitable for high temperature structural applications unless one could

significantly increase T_g and T_x and design the so-called high temperature MGs, as discussed in [19].

5. Summary

To sum up, we provide an overview in this work on the recent development of chemically complex MGs by focusing on the new methods for alloy design, AM, and some new and interesting applications. Since the 1960s, people have developed over 5000 MG compositions including over 800 BMGs. However, with the approach of big data, we expect that one could discover and develop more new MG compositions with excellent GFAs at a much faster pace with higher efficiency. Putting aside GFAs, AM provides an alternative way to produce bulk sized MGs for industrial applications. After 30 year continuous development, we now have a variety of AM methods established based on the principle of either hot or cold fusion. Compared to cast MGs, manufactured MGs are not restricted in size and geometry by their GFAs, therefore more amenable to structural and functional applications. With these new tools and developments, we anticipate that one may face another surge of renewed interest in chemically complex MGs in near future over a very wide range of applications.

Acknowledgments

Y Y acknowledges financial support provided by the Research Grants Committee (RGC), the Hong Kong government, the General Research Fund (GRF) with Grant Nos. CityU11200719 and CityU11213118, and also by the City University of Hong Kong through an internal grant with Grant No. 7005438.

ORCID iD

Y Yang https://orcid.org/0000-0002-0491-8295

References

[1] Kramer J 1937 Der amorphe Zustand der Metalle *Z. Phys.* **106** 675–91
[2] Brenner A, Couch D E and Williams E K 1950 Electrodeposition of alloys of phosphorus with nickel or cobalt *J. Res. Natl Bur. Stand.* **44** 109
[3] Klement W, Willens R and Duwez P 1960 Non-crystalline structure in solidified gold–silicon alloys *Nature* **187** 869–70
[4] Chen H S and Turnbull D 1968 Evidence of a glass-liquid transition in a gold-germanium-silicon alloy *J. Chem. Phys.* **48** 2560–71
[5] Chen H S 1974 Thermodynamic considerations on the formation and stability of metallic glasses *Acta Metall.* **22** 1505–11
[6] Kui H W, Greer A L and Turnbull D 1984 Formation of bulk metallic glass by fluxing *Appl. Phys. Lett.* **45** 615–6
[7] Inoue A, Zhang T and Masumoto T 1990 Production of amorphous cylinder and sheet of La55Al25Ni20 alloy by a metallic mold casting method *Mater. Trans. JIM* **31** 425–8
[8] Inoue A, Zhang T and Masumoto T 1990 Zr-Al-Ni amorphous alloys with high glass transition temperature and significant supercooled liquid region *Mater. Trans. JIM* **31** 177–83
[9] Peker A and Johnson W L 1993 A highly processable metallic glass: zr41.2Ti13.8Cu12.5Ni10.0Be22.5 *Appl. Phys. Lett.* **63** 2342–4
[10] Lindsay Greer A 1993 Confusion by design *Nature* **366** 303–4
[11] Inoue A 2000 Stabilization of metallic supercooled liquid *Acta Mater.* **48** 279–306
[12] Suryanarayana C and Inoue A 2011 *Bulk Metallic Glasses* (Boca Raton, FL: CRC Press) (n.d.) (https://doi.org/10.1201/9781315153483)
[13] Luo Q and Wang W H 2009 Rare earth based bulk metallic glasses *J. Non-Cryst. Solids* **355** 759–75
[14] Tang M B, Bai H Y, Pan M X, Zhao D Q and Wang W H 2005 Bulk metallic superconductive La60Cu20Ni 10Al10 glass *J. Non-Cryst. Solids* **351** 2572–5
[15] Zhang B, Pan M X, Zhao D Q and Wang W H 2004 'Soft' bulk metallic glasses based on cerium *Appl. Phys. Lett.* **85** 61–3
[16] Zhao Z F, Zhang Z, Wen P, Pan M X, Zhao D Q, Wang W H and Wang W L 2003 A highly glass-forming alloy with low glass transition temperature *Appl. Phys. Lett.* **82** 4699–701
[17] Zhou Z Q, He Q F, Liu X D, Wang Q, Luan J H, Liu C T and Yang Y 2021 Rational design of chemically complex metallic glasses by hybrid modeling guided machine learning *npj Comput. Mater.* **7** 1–10
[18] Ding S, Liu Y, Li Y, Liu Z, Sohn S, Walker F J and Schroers J 2014 Combinatorial development of bulk metallic glasses *Nat. Mater.* **13** 494–500
[19] Li M X, Zhao S F, Lu Z, Hirata A, Wen P, Bai H Y, Chen M W, Schroers J, Liu Y H and Wang W H 2019 High-temperature bulk metallic glasses developed by combinatorial methods *Nature* **569** 99–103
[20] Ward L, Agrawal A, Choudhary A and Wolverton C 2016 A general-purpose machine learning framework for predicting properties of inorganic materials *npj Comput. Mater.* **2** 1–7
[21] Yoshida S, Mizushima T, Makino A and Inoue A 1999 Structure and soft magnetic properties of bulk Fe-based glassy alloy prepared by pulse current sintering *Nippon Kinzoku Gakkaishi/J. Japan Inst. Met.* **63** 1097–100
[22] Ishihara S, Zhang W, Kimura H, Omori M and Inoue A 2003 Consolidation of Fe-Co-Nd-Dy-B glassy powders by spark-plasma sintering and magnetic properties of the consolidated alloys *Mater. Trans.* **44** 138–43
[23] Pauly S, Löber L, Petters R, Stoica M, Scudino S, Kühn U and Eckert J 2013 Processing metallic glasses by selective laser melting *Mater. Today* **16** 37–41
[24] Zhang C, Ouyang D, Pauly S and Liu L 2021 3D printing of bulk metallic glasses *Mater. Sci. Eng.* R **145** 100625
[25] Kawamura Y and Ohno Y 2001 Superplastic bonding of bulk metallic glasses using friction *Scr. Mater.* **45** 279–85
[26] Kawamura Y, Shoji T and Ohno Y 2003 Welding technologies of bulk metallic glasses *J. Non-Cryst. Solids* **317** 152–7
[27] Kagao S, Kawamura Y and Ohno Y 2004 Electron-beam welding of Zr-based bulk metallic glasses *Mater. Sci. Eng.* A **375–377** 312–6
[28] Kawamura Y and Ohno Y 2001 Successful electron-beam welding of bulk metallic glass *Mater. Trans.* **42** 2476–8
[29] Kawamura Y 2004 Liquid phase and supercooled liquid phase welding of bulk metallic glasses *Mater. Sci. Eng.* A **375–377** 112–9

[30] Li B, Li Z Y, Xiong J G, Xing L, Wang D and Li Y 2006 Laser welding of Zr45Cu48Al7 bulk glassy alloy *J. Alloys Compd.* **413** 118–21

[31] Chiba A, Kawamura Y and Nishida M 2008 Explosive welding of ZrTiCuNiBe bulk metallic glass to crystalline metallic plates *Materials Science Forum* (Trans Tech Publications Ltd) **556** 119–24

[32] Kawamura Y and Ohno Y 2001 Spark welding of Zr55Al10Ni5Cu30 bulk metallic glasses *Scr. Mater.* **45** 127–32

[33] Chen W, Liu Z and Schroers J 2014 Joining of bulk metallic glasses in air *Acta Mater.* **62** 49–57

[34] Ma J *et al* 2019 Fast surface dynamics enabled cold joining of metallic glasses *Sci. Adv.* **5** eaax7256

[35] Kawamura Y, Takagi M, Senoo M and Imura T 1988 Preparation of bulk amorphous alloys by high temperature sintering under a high pressure *Mater. Sci. Eng.* **98** 415–8

[36] Kawamura Y, Inoue A, Sasamori K and Masumoto T 1994 Consolidation mechanism of aluminum-based amorphous alloy powders during warm extrusion *Mater. Sci. Eng.* A **181–182** 1174–8

[37] Kawamura Y, Kato H, Inoue A and Masumoto T 1995 Full strength compacts by extrusion of glassy metal powder at the supercooled liquid state *Appl. Phys. Lett.* **67** 2008

[38] Xie G, Zhang W, Louzguine-Luzgin D V, Kimura H and Inoue A 2006 Fabrication of porous Zr-Cu-Al-Ni bulk metallic glass by spark plasma sintering process *Scr. Mater.* **55** 687–90

[39] Wang D J, Huang Y J, Shen J, Wu Y Q, Huang H and Zou J 2010 Temperature influence on sintering with concurrent crystallization behavior in Ti-based metallic glassy powders *Mater. Sci. Eng.* A **527** 2662–8

[40] Xie G, Louzguine-Luzgin D V, Kimura H and Inoue A 2007 Nearly full density Ni52.5 Nb10 Zr15 Ti15 Pt7.5 bulk metallic glass obtained by spark plasma sintering of gas atomized powders *Appl. Phys. Lett.* **90** 3–5

[41] Sun H and Flores K M 2008 Laser deposition of a Cu-based metallic glass powder on a Zr-based glass substrate *J. Mater. Res.* **23** 2692–703

[42] Wang Q, Liu J J, Ye Y F, Liu T T, Wang S, Liu C T, Lu J and Yang Y 2017 Universal secondary relaxation and unusual brittle-to-ductile transition in metallic glasses *Mater. Today* **20** 293–300

[43] Cann J L *et al* 2021 Sustainability through alloy design: challenges and opportunities *Prog. Mater. Sci.* **117** 100722

[44] Kennedy B W 1998 *Energy Efficient Transformers* (McGraw Hill Professional) (New York: City) (available at: https://books.google.com.bn/books?id=_CcC0q-9ie0C&hl=ms&source=gbs_navlinks_s)

[45] Kaushik N, Sharma P, Ahadian S, Khademhosseini A, Takahashi M, Makino A, Tanaka S and Esashi M 2014 Metallic glass thin films for potential biomedical applications *J. Biomed. Mater. Res.* B **102** 1544–52

[46] Li H F and Zheng Y F 2016 Recent advances in bulk metallic glasses for biomedical applications *Acta Biomater.* **36** 1–20

[47] Chu J P *et al* 2012 Thin film metallic glasses: unique properties and potential applications *Thin Solid Films* **520** 5097–122

[48] Yang C, Zhang C, Xing W and Liu L 2018 3D printing of Zr-based bulk metallic glasses with complex geometries and enhanced catalytic properties *Intermetallics* **94** 22–8

[49] Tan Y, Zhu F, Wang H, Tian Y, Hirata A, Fujita T and Chen M 2017 Noble-metal-free metallic glass as a highly active and stable bifunctional electrocatalyst for water splitting *Adv. Mater. Interfaces* **4** 1601086

[50] Wu K, Meng Y, Li X, Ma J, Zhang P, Li W, Huo L and Lin H J 2020 Improved alkaline hydrogen evolution performance of a Fe78Si9B13 metallic glass electrocatalyst by ultrasonic vibrations *Intermetallics* **125** 106820

[51] Turnbull D 1969 Under what conditions can a glass be formed? *Contemp. Phys.* **10** 473–88

[52] Shintani H and Tanaka H 2006 Frustration on the way to crystallization in glass *Nat. Phys.* **2** 200–6

[53] Ma D, Tan H, Wang D, Li Y and Ma E 2005 Strategy for pinpointing the best glass-forming alloys *Appl. Phys. Lett.* **86** 1–3

[54] Wang D, Tan H and Li Y 2005 Multiple maxima of GFA in three adjacent eutectics in Zr-Cu-Al alloy system—a metallographic way to pinpoint the best glass forming alloys *Acta Mater.* **53** 2969–79

[55] Dai C L, Guo H, Li Y and Xu J 2008 A new composition zone of bulk metallic glass formation in the Cu-Zr-Ti ternary system and its correlation with the eutectic reaction *J. Non-Cryst. Solids* **354** 3659–65

[56] Wang Q, Liu C T, Yang Y, Dong Y D and Lu J 2011 Atomic-scale structural evolution and stability of supercooled liquid of a Zr-based bulk metallic glass *Phys. Rev. Lett.* **106** 215505

[57] Wang W H 2014 High-entropy metallic glasses *JOM* **66** 2067–77

[58] Wada T, Jiang J, Yubuta K, Kato H and Takeuchi A 2019 Septenary Zr–Hf–Ti–Al–Co–Ni–Cu high-entropy bulk metallic glasses with centimeter-scale glass-forming ability *Materialia* **7** 3–8

[59] Gao X Q, Zhao K, Ke H B, Ding D W, Wang W H and Bai H Y 2011 High mixing entropy bulk metallic glasses *J. Non-Cryst. Solids* **357** 3557–60

[60] Zhao S F, Shao Y, Liu X, Chen N, Ding H Y and Yao K F 2015 Pseudo-quinary Ti20Zr20Hf20Be20(Cu20-xNix) high entropy bulk metallic glasses with large glass forming ability *Mater. Des.* **87** 625–31

[61] Ding H Y, Shao Y, Gong P, Li J F and Yao K F 2014 A senary TiZrHfCuNiBe high entropy bulk metallic glass with large glass-forming ability *Mater. Lett.* **125** 151–3

[62] Takeuchi A, Chen N, Wada T, Yokoyama Y, Kato H, Inoue A and Yeh J W 2011 Pd20Pt20Cu20Ni20P20 high-entropy alloy as a bulk metallic glass in the centimeter *Intermetallics* **19** 1546–54

[63] Ding H Y and Yao K F 2013 High entropy Ti20Zr20Cu20Ni 20Be20 bulk metallic glass *J. Non-Cryst. Solids* **364** 9–12

[64] Li Y, Guo Q, Kalb J A and Thompson C V 2008 Matching glass-forming ability with the density of the amorphous phase *Science* **322** 1816–9

[65] Ding S, Gregoire J, Vlassak J J and Schroers J 2012 Solidification of Au-Cu-Si alloys investigated by a combinatorial approach *J. Appl. Phys.* **111** 114901

[66] Ren F, Ward L, Williams T, Laws K J, Wolverton C, Hattrick-Simpers J and Mehta A 2018 Accelerated discovery of metallic glasses through iteration of machine learning and high-throughput experiments *Sci. Adv.* **4** eaaq1566

[67] Tsai P and Flores K M 2016 High-throughput discovery and characterization of multicomponent bulk metallic glass alloys *Acta Mater.* **120** 426–34

[68] Tsai P and Flores K M 2014 A combinatorial strategy for metallic glass design via laser deposition *Intermetallics* **55** 162–6

[69] Inoue A, Shinohara Y, Yokoyama Y and Masumoto T 1995 Solidification analyses of bulky Zr-Al-Ni-Cu-Pd glass produced by casting wedge-shape copper mold *Mater. Trans. JIM* **36** 1276–81

[70] Laws K J, Gun B and Ferry M 2009 Influence of casting parameters on the critical casting size of bulk metallic glass *Metall. Mater. Trans.* A **40** 2377–87

[71] Liu X, Li X, He Q, Liang D, Zhou Z, Ma J, Yang Y and Shen J 2020 Machine learning-based glass formation prediction in multicomponent alloys *Acta Mater.* **201** 182–90

[72] Li M and Flores K M 2020 Laser processing as a high-throughput method to investigate microstructure-processing-property relationships in multiprincipal element alloys *J. Alloys Compd.* **825** 154025

[73] Tripathi M K, Chattopadhyay P P and Ganguly S 2015 Multivariate analysis and classification of bulk metallic glasses using principal component analysis *Comput. Mater. Sci.* **107** 79–87

[74] Xiong J, Zhang T Y and Shi S Q 2019 Machine learning prediction of elastic properties and glass-forming ability of bulk metallic glasses *MRS Commun.* **9** 576–85

[75] Xiong J, Shi S-Q and Zhang T-Y 2019 A machine-learning approach to predicting and understanding the properties of amorphous metallic alloys *Mater. Des.* **187** 108378

[76] Ward L, O'Keeffe S C, Stevick J, Jelbert G R, Aykol M and Wolverton C 2018 A machine learning approach for engineering bulk metallic glass alloys *Acta Mater.* **159** 102–11

[77] Cai A H, Xiong X, Liu Y, An W K and Tan J Y 2008 Artificial neural network modeling of reduced glass transition temperature of glass forming alloys *Appl. Phys. Lett.* **92** 10–3

[78] Sun Y T, Bai H Y, Li M Z and Wang W H 2017 Machine learning approach for prediction and understanding of glass-forming ability *J. Phys. Chem. Lett.* **8** 3434–9

[79] Zhou Z, Zhou Y, He Q, Ding Z, Li F and Yang Y 2019 Machine learning guided appraisal and exploration of phase design for high entropy alloys *npj Comput. Mater.* **5** 1–9

[80] Butler K T, Davies W, Cartwright H, Isayev O and Walsh A 2018 Review machine learning for molecular and materials science *Nature* **559** 547–55

[81] Hart G L W, Mueller T, Toher C and Curtarolo S 2021 Machine learning for alloys *Nat. Rev. Mater.* **6** 730–55

[82] Kawazoe Y, Carow-Watamura U and Louzguine D V 1997 *Phase Diagrams and Physical Properties of Nonequilibrium Alloys* (Springer-Verlag Berlin and Heidelberg GmbH & Co. KG; Publisher location: Berlin, Germany) (https://doi.org/10.1007/b58222)

[83] Kawazoe Y 1997 Nonequilibrium phase diagrams of ternary amorphous alloys **37** 1–129

[84] Long Z, Wei H, Ding Y, Zhang P, Xie G and Inoue A 2009 A new criterion for predicting the glass-forming ability of bulk metallic glasses *J. Alloys Compd.* **475** 207–19

[85] Dasgupta A, Broderick S R, Mack C, Kota B U, Subramanian R, Setlur S, Govindaraju V and Rajan K 2019 Probabilistic assessment of glass forming ability rules for metallic glasses aided by automated analysis of phase diagrams *Sci. Rep.* **9** 1–12

[86] Senkov O N, Miller J D, Miracle D B and Woodward C 2015 Accelerated exploration of multi-principal element alloys for structural applications *CALPHAD, Comput. Coupling Phase Diagr.* **50** 32–48

[87] Samavatian M, Gholamipour R and Samavatian V 2021 Discovery of novel quaternary bulk metallic glasses using a developed correlation-based neural network approach *Comput. Mater. Sci.* **186** 110025

[88] Ren B, Long Z and Deng R 2021 A new criterion for predicting the glass-forming ability of alloys based on machine learning *Comput. Mater. Sci.* **189** 110259

[89] Cai A H, Liu Y, An W K, Zhou G J, Luo Y, Li T L, Li X S and Tan X F 2013 Prediction of critical cooling rate for glass forming alloys by artificial neural network *Mater. Des.* **52** 671–6

[90] Deng B and Zhang Y 2020 Critical feature space for predicting the glass forming ability of metallic alloys revealed by machine learning *Chem. Phys.* **538** 110898

[91] Mastropietro D G and Moya J A 2021 Design of Fe-based bulk metallic glasses for maximum amorphous diameter (Dmax) using machine learning models *Comput. Mater. Sci.* **188** 110230

[92] Majid A, Ahsan S B and Tariq N U H 2015 Modeling glass-forming ability of bulk metallic glasses using computational intelligent techniques *Appl. Soft Comput. J.* **28** 569–78

[93] Ghiringhelli L M, Vybiral J, Levchenko S V, Draxl C and Scheffler M 2015 Big data of materials science: critical role of the descriptor *Phys. Rev. Lett.* **114** 105503

[94] Zhang Y and Ling C 2018 A strategy to apply machine learning to small datasets in materials science *npj Comput. Mater.* **4** 28–33

[95] Ishihara S, Zhang W and Inoue A 2002 Hot pressing of Fe-Co-Nd-Dy-B glassy powders in supercooled liquid state and hard magnetic properties of the consolidated alloys *Scr. Mater.* **47** 231–5

[96] Sun Y, Concustell A and Greer A L 2016 Thermomechanical processing of metallic glasses: extending the range of the glassy state *Nat. Rev. Mater.* **1** 1–14

[97] Somekawa H, Inoue A and Higashi K 2004 Superplastic and diffusion bonding behavior on Zr-Al-Ni-Cu metallic glass in supercooled liquid region *Scr. Mater.* **50** 1395–9

[98] Kuo P H, Wang S H, Liaw P K, Fan G J, Tsang H T, Qiao D and Jiang F 2010 Bulk-metallic glasses joining in a supercooled-liquid region *Mater. Chem. Phys.* **120** 532–6

[99] Choi P P, Kim J S, Nguyen O T H, Kwon D H, Kwon Y S and Kim J C 2007 Al-La-Ni-Fe bulk metallic glasses produced by mechanical alloying and spark-plasma sintering *Mater. Sci. Eng.* A **449–451** 1119–22

[100] Cardinal S, Pelletier J M, Qiao J C, Bonnefont G and Xie G 2016 Influence of spark plasma sintering parameters on the mechanical properties of Cu50Zr45Al5 bulk metallic glass obtained using metallic glass powder *Mater. Sci. Eng.* A **677** 116–24

[101] Zheng B, Ashford D, Zhou Y, Mathaudhu S N, Delplanque J P and Lavernia E J 2013 Influence of mechanically milled powder and high pressure on spark plasma sintering of Mg-Cu-Gd metallic glasses *Acta Mater.* **61** 4414–28

[102] Munir Z A, Anselmi-Tamburini U and Ohyanagi M 2006 The effect of electric field and pressure on the synthesis and consolidation of materials: a review of the spark plasma sintering method *J. Mater. Sci.* **41** 763–77

[103] Kelly J P, Fuller S M, Seo K, Novitskaya E, Eliasson V, Hodge A M and Graeve O A 2016 Designing *in situ* and ex situ bulk metallic glass composites via spark plasma sintering in the super cooled liquid state *Mater. Des.* **93** 26–38

[104] Kim C K, Lee S, Shin S Y and Kim D H 2008 Effects of consolidation temperature and pressure on microstructures and mechanical properties of Cu-based bulk amorphous alloys consolidated by spark plasma sintering *J. Alloys Compd.* **453** 108–14

[105] Shoji T, Kawamura Y and Ohno Y 2004 Friction welding of bulk metallic glasses to different ones *Mater. Sci. Eng.* A **375–377** 394–8

[106] Shin H S, Jeong Y J, Choi H Y, Kato H and Inoue A 2007 Joining of Zr-based bulk metallic glasses using the friction welding method *J. Alloys Compd.* **434–435** 102–5

[107] Ohkubo T, Shoji S, Kawamura Y and Hono K 2005 Nanostructure analysis of friction welded Pd-Ni-P/Pd-Cu-Ni-P metallic glass interface *Scr. Mater.* **53** 493–7

[108] Sun Y, Ji Y, Fujii H, Nakata K and Nogi K 2010 Microstructure and mechanical properties of friction stir welded joint of Zr55Cu30Al10Ni5 bulk metallic glass with pure copper *Mater. Sci. Eng.* A **527** 3427–32

[109] Jamili-Shirvan Z, Haddad-Sabzevar M, Vahdati-Khaki J, Chen N, Shi Q and Yao K F 2016 Microstructure characterization and mechanical properties of Ti-based bulk metallic glass joints prepared with friction stir spot welding process *Mater. Des.* **100** 120–31

[110] Liu Z, Chen W, Carstensen J, Ketkaew J, Mota R M O, Guest J K and Schroers J 2016 3D metallic glass cellular structures *Acta Mater.* **105** 35–43

[111] Peng Q, Xie Y, Zhu B, Chen W, Schroers J, Chen M and Liu Z 2020 Joining mechanism of bulk metallic glasses in their supercooled liquid region *J. Mater. Process. Technol.* **279** 116583

[112] Pauly S, Schricker C, Scudino S, Deng L and Kühn U 2017 Processing a glass-forming Zr-based alloy by selective laser melting *Mater. Des.* **135** 133–41

[113] Ouyang D, Xing W, Li N, Li Y and Liu L 2018 Structural evolutions in 3D-printed Fe-based metallic glass fabricated by selective laser melting *Addit. Manuf.* **23** 246–52

[114] Jung H Y, Choi S J, Prashanth K G, Stoica M, Scudino S, Yi S, Kühn U, Kim D H, Kim K B and Eckert J 2015 Fabrication of Fe-based bulk metallic glass by selective laser melting: a parameter study *Mater. Des.* **86** 703–8

[115] Ouyang D, Li N, Xing W, Zhang J and Liu L 2017 3D printing of crack-free high strength Zr-based bulk metallic glass composite by selective laser melting *Intermetallics* **90** 128–34

[116] Li N, Zhang J, Xing W, Ouyang D and Liu L 2018 3D printing of Fe-based bulk metallic glass composites with combined high strength and fracture toughness *Mater. Des.* **143** 285–96

[117] Yang C, Zhang C and Liu L 2018 Excellent degradation performance of 3D hierarchical nanoporous structures of copper towards organic pollutants *J. Mater. Chem.* A **6** 20992–1002

[118] Zhang C, Li X-M, Liu S-Q, Liu H, Yu L-J and Liu L 2019 3D printing of Zr-based bulk metallic glasses and components for potential biomedical applications *J. Alloys Compd.* **790** 963–73

[119] Nicholas E D 2003 Friction processes technologies *Weld. World* **47** 2–9

[120] Uday M B, Fauzi M N A, Zuhailawati H and Ismail A B 2010 Advances in friction welding process: a review *Sci. Technol. Weld. Join.* **15** 534–58

[121] Schroers J 2005 The superplastic forming of bulk metallic glasses *JOM* **57** 35–39

[122] Schroers J 2010 Processing of bulk metallic glass *Adv. Mater.* **22** 1566–97

[123] Swiston A J, Hufnagel T C and Weihs T P 2003 Joining bulk metallic glass using reactive multilayer foils *Scr. Mater.* **48** 1575–80

[124] Guo S F, Chan K C, Zhu Z Q, Wu Z R, Chen W and Song M 2016 Microstructure and tensile behavior of small scale resistance spot welding of sandwich bulk metallic glasses *J. Non-Cryst. Solids* **447** 300–6

[125] Liu L H, Yang C, Kang L M, Qu S G, Li X Q, Zhang W W, Chen W P, Li Y Y, Li P J and Zhang L C 2016 A new insight into high-strength Ti62Nb12.2Fe13.6Co6.4Al5.8 alloys with bimodal microstructure fabricated by semi-solid sintering *Sci. Rep.* **6** 1–7

[126] Kawamura Y, Kagao S and Ohno Y 2001 Electron beam welding of Zr-based bulk metallic glass to crystalline Zr metal *Mater. Trans.* **42** 2649–51

[127] Hanliang L, Ning L, Xiaojie L, Xin S, Tao S and Zhanguo M 2019 Joining of Zr60Ti17Cu12Ni11 bulk metallic glass and aluminum 1060 by underwater explosive welding method *J. Manuf. Process.* **45** 115–22

[128] Kawamura Y, Ohno Y and Chiba A 2002 Development of welding technologies in bulk metallic glasses *J. Metastable Nanocryst. Mater.* **13** 553–8

[129] Liu K X, Liu W D, Wang J T, Yan H H, Li X J, Huang Y J, Wei X S and Shen J 2008 Atomic-scale bonding of bulk metallic glass to crystalline aluminum *Appl. Phys. Lett.* **93** 13–16

[130] Jiang M Q, Huang B M, Jiang Z J, Lu C and Dai L H 2015 Joining of bulk metallic glass to brass by thick-walled cylinder explosion *Scr. Mater.* **97** 17–20

[131] Williams E and Lavery N 2017 Laser processing of bulk metallic glass: a review *J. Mater. Process. Technol.* **247** 73–91

[132] Kim J, Lee D, Shin S and Lee C 2006 Phase evolution in Cu54Ni6Zr22Ti18 bulk metallic glass Nd: YAGlaser weld *Mater. Sci. Eng.* A **434** 194–201

[133] Kawahito Y, Terajima T, Kimura H, Kuroda T, Nakata K, Katayama S and Inoue A 2008 High-power fiber laser welding and its application to metallic glass Zr55Al10Ni5Cu30 *Mater. Sci. Eng.* B **148** 105–9

[134] Shao L, Datye A, Huang J, Ketkaew J, Sohn S W, Zhao S, Wu S, Zhang Y, Schwarz U D and Schroers J 2017 Pulsed laser beam welding of Pd43Cu27Ni10P20 bulk metallic glass *Sci. Rep.* **7** 1–7

[135] Li J F, Sun Y H, Ding D W, Wang W H and Bai H Y 2020 Nanosecond-pulsed laser welding of metallic glass *J. Non-Cryst. Solids* **537** 120016

[136] Wang G, Huang Y J, Shagiev M and Shen J 2012 Laser welding of Ti 40Zr 25Ni 3Cu 12Be 20 bulk metallic glass *Mater. Sci. Eng.* A **541** 33–7

[137] Sohrabi N, Jhabvala J and Logé R E 2021 Additive manufacturing of bulk metallic glasses—process, challenges and properties: a review *Metals* **11** 1279

[138] Katakam S, Hwang J Y, Paital S, Banerjee R, Vora H and Dahotre N B 2012 *In situ* laser synthesis of Fe-based amorphous matrix composite coating on structural steel *Metall. Mater. Trans.* A **43** 4957–66

[139] Herzog D, Seyda V, Wycisk E and Emmelmann C 2016 Additive manufacturing of metals *Acta Mater.* **117** 371–92

[140] Liu H, Jiang Q, Huo J, Zhang Y, Yang W and Li X 2020 Crystallization in additive manufacturing of metallic glasses: a review *Addit. Manuf.* **36** 101568

[141] Li Z, Huang Z, Sun F, Li X and Ma J 2020 Forming of metallic glasses: mechanisms and processes *Mater. Today Adv.* **7** 100077

[142] Li Z and Ma J 2021 Water-repellent surfaces of metallic glasses: fabrication and application *Mater. Today Adv.* **12** 100164

[143] Liang X, Zhu X, Li X, Mo R, Liu Y, Wu K and Ma J 2020 High-entropy alloy and amorphous alloy composites fabricated by ultrasonic vibrations *Sci. China Phys. Mech. Astron.* **63** 1–5

[144] Sun F, Wang B, Luo F, Yan Y Q, Ke H B, Ma J, Shen J and Wang W H 2020 Shear punching of bulk metallic glasses under low stress *Mater. Des.* **190** 108595

[145] Sohrabi S, Li M X, Bai H Y, Ma J, Wang W H and Greer A L 2020 Energy storage oscillation of metallic glass induced by high-intensity elastic stimulation *Appl. Phys. Lett.* **116** 81901

[146] Yuan C, Lv Z, Pang C, Li X, Liu R, Yang C, Ma J, Ke H, Wang W and Shen B 2021 Ultrasonic-assisted plastic flow in a Zr-based metallic glass *Sci. China Mater.* **64** 448–59

[147] Li X *et al* 2020 Ultrasonic plasticity of metallic glass near room temperature *Appl. Mater. Today* **21** 100866

[148] Li H, Yan Y, Sun F, Li K, Luo F and Ma J 2019 Shear punching of amorphous alloys under high-frequency vibrations *Metals* **9** 1158

[149] Luo F, Sun F, Li K, Gong F, Liang X, Wu X and Ma J 2018 Ultrasonic assisted micro-shear punching of amorphous alloy *Mater. Res. Lett.* **6** 545–51

[150] Li X, Liang X, Zhang Z, Ma J and Shen J 2020 Cold joining to fabricate large size metallic glasses by the ultrasonic vibrations *Scr. Mater.* **185** 100–4

[151] Huang Z, Fu J, Li X, Wen W, Lin H, Lou Y, Luo F, Zhang Z, Liang X and Ma J 2021 Ultrasonic-assisted rapid cold welding of bulk metallic glasses *Sci. China Mater.* **64** 1–8

[152] Ma L, Wang L, Zhang T and Inoue A 2002 Bulk glass formation of Ti-Zr-Hf-Cu-M (M=Fe, Co, Ni) alloys *Mater. Trans.* **43** 277–80

[153] Yeh J W, Chen S K, Lin S J, Gan J Y, Chin T S, Shun T T, Tsau C H and Chang S Y 2004 Nanostructured high-entropy alloys with multiple principal elements: novel alloy design concepts and outcomes *Adv. Eng. Mater.* **6** 299–303

[154] Cantor B, Chang I T H, Knight P and Vincent A J B 2004 Microstructural development in equiatomic multicomponent alloys *Mater. Sci. Eng.* A **375–377** 213–8

[155] Yang M, Liu X J, Wu Y, Wang H, Jiang S H, Wang X Z and Lu Z P 2020 Research progress on high-entropy bulk metallic glasses *Sci. Sin. Phys. Mech. Astron.* **50** 067003

[156] Wu K, Liu C, Li Q, Huo J, Li M, Chang C and Sun Y 2019 Magnetocaloric effect of Fe25Co25Ni25Mo5P10B10 high-entropy bulk metallic glass *J. Magn. Magn. Mater.* **489** 165404

[157] Huo J, Huo L, Li J, Men H, Wang X, Inoue A, Chang C, Wang J Q and Li R W 2015 High-entropy bulk metallic glasses as promising magnetic refrigerants *J. Appl. Phys.* **117** 073902

[158] Li J, Xue L, Yang W, Yuan C, Huo J and Shen B 2018 Distinct spin glass behavior and excellent magnetocaloric effect in Er20Dy20Co20Al20RE20 (RE = Gd, Tb and Tm) high-entropy bulk metallic glasses *Intermetallics* **96** 90–3

[159] Huo J T, Zhao D Q, Bai H Y, Axinte E and Wang W H 2013 Giant magnetocaloric effect in Tm-based bulk metallic glasses *J. Non-Cryst. Solids* **359** 1–4

[160] Ray R and Musso E 1976 *Amorphous Alloys in the U-Cr-V System* (available at: https://patents.google.com/patent/US3981722A/en)

[161] Elliott R O and Giessen B C 1982 On the formation of metallic glasses based on U, Np or Pu *Acta Metall.* **30** 785–9

[162] Drehman A J and Poon S J 1985 Anomalous glass-forming ability of uranium-based alloys *J. Non-Cryst. Solids* **76** 321–32

[163] Huang H, Zhang P G, Ke H, Zhang P and Liu T 2016 Progress of uranium-contain amorphous alloy *Mater. Rep.* **30** 564–7 (available at: http://222.198.130.40:81/Qikan/Article/Detail?id=670790822)

[164] Zhang P, Pu Z, Zhang P, Huang H, Cai D and Wang Y 2020 U-Fe-Al metallic glasses with superior glass forming ability and corrosion resistance *J. Mater. Res. Technol.* **9** 6209–16

[165] Ke H B, Zhang P, Sun B A, Zhang P G, Liu T W, Chen P H, Wu M and Huang H G 2019 Dissimilar nanoscaled structural heterogeneity in U-based metallic glasses revealed by nanoindentation *J. Alloys Compd.* **788** 391–6

[166] Huang H G, Wang Y M, Chen L, Pu Z, Zhang P G and Liu T W 2015 Study on formation and corrosion resistance of amorphous alloy in U-Co system *Acta Met. Sin.* **51** 623

[167] Zhang L, Yi T, Huang H-G, Zhang P, Zhang F-G, Wu M and Fa C 2021 Phase separation and solidification sequence of uranium-based amorphous composites *Acta Met. Sin.* **57** 0

[168] Han L-H, Ke H-B, Zhang P, Sang G and Huang H-G 2021 Kinetic crystallization behavior of amorphous U60Fe27. 5Al12. 5 alloy *Acta Met. Sin.* **57** 0

[169] Huang H, Zhang P, Zhang P and Wang Q 2020 Comparison of glass forming ability between U-Co and U-Fe base systems *Acta Metall. Sin.* **56** 849–54

[170] Xu H, Ke H, Huang H, Zhang P, Zhang P and Liu T 2017 Nanoindentation creep behavior of U65Fe30Al5 amorphous alloy *Acta Metall. Sin.* **53** 817–23

[171] Ke H B, Pu Z, Zhang P, Zhang P G, Xu H Y, Huang H G, Liu T W and Wang Y M 2017 Research progress in U-based amorphous alloys *Acta Phys. Sin.* **66** 176104

[172] Huang H, Ke H, Zhang P and Zhang P 2019 U-based binary strong glass forming system *J. Non-Cryst. Solids* **511** 68–75

[173] Xu H, Ke H, Huang H, Zhang P, Pu Z, Zhang P and Liu T 2018 U-based metallic glasses with superior glass forming ability *J. Nucl. Mater.* **499** 372–6

[174] Huang H, Ke H, Zhang P, Pu Z, Zou D, Zhang P, Shi T, Zhang L and Liu T 2018 U-involved sphere-dispersed metallic glass matrix composites *Mater. Des.* **157** 371–6

[175] Huogen H, Haibo K, Tianwei L, Pengguo Z, Xiane T and Yingmin W 2018 Effect of minor alloying on the glass forming ability of U-Co alloy *RARE Met. Mater. Eng.* **47** 990–4 (available at: www.rmme.ac.cn/rmme/ch/reader/view_abstract.aspx?journal_id=rmme&file_no=20160075&html_url=rmme/article/html/20160075)

[176] Ke H B, Xu H Y, Huang H G, Liu T W, Zhang P, Wu M, Zhang P G and Wang Y M 2017 Non-isothermal crystallization behavior of U-based amorphous alloy *J. Alloys Compd.* **691** 436–41

[177] Huang H, Xu H, Zhang P, Wang Y, Ke H, Zhang P and Liu T 2016 U-Cr binary alloys with anomalous glass-forming ability *Acta Met. Sin.* **53** 233–8

[178] Huang H G, Ke H B, Zhang P, Wang Y M, Zhang P G, Wu M and Liu T W 2016 Effect of minor alloying on the glass formation of U-based alloys *J. Alloys Compd.* **688** 599–604

[179] Huang H G, Ke H B, Wang Y M, Pu Z, Zhang P, Zhang P G and Liu T W 2016 Stable U-based metallic glasses *J. Alloys Compd.* **684** 75–83

[180] Villapún V M, Dover L G, Cross A and González S 2016 Antibacterial metallic touch surfaces *Materials* **9** 736

[181] Lin B, Mu R, Yang L and Bian X 2012 Antibacterial effect of metallic glasses *Chin. Sci. Bull.* **57** 1069–72

[182] Villapún V M, Zhang H, Howden C, Chow L C, Esat F, Pérez P, Sort J, Bull S, Stach J and González S 2017 Antimicrobial and wear performance of Cu-Zr-Al metallic glass composites *Mater. Des.* **115** 93–102

[183] Chu J P, Liu T Y, Li C L, Wang C H, Jang J S C, Chen M J, Chang S H and Huang W C 2014 Fabrication and characterizations of thin film metallic glasses: antibacterial property and durability study for medical application *Thin Solid Films* **561** 102–7

[184] Gadi B and Jeffrey G 2005 Copper as a biocidal tool *Curr. Med. Chem.* **12** 2163–75

[185] Grass G, Rensing C and Solioz M 2011 Metallic copper as an antimicrobial surface *Appl. Environ. Microbiol.* **77** 1541–7

[186] Villapún V M, Qu B, Lund P A, Wei W, Dover L G, Thompson J R, Adesina J O, Hoerdemann C, Cox S and González S 2020 Optimizing the antimicrobial performance of metallic glass composites through surface texturing *Mater. Today Commun.* **23** 101074

[187] Villapún V M, Tardío S, Cumpson P, Burgess J G, Dover L G and González S 2019 Antimicrobial properties of Cu-based bulk metallic glass composites after surface modification *Surf. Coat. Technol.* **372** 111–20

[188] Villapún V M, Esat F, Bull S, Dover L G and Gonzalez S 2017 Tuning the mechanical and antimicrobial

performance of a Cu-based metallic glass composite through cooling rate control and annealing *Materials* **10** 506
[189] El-Eskandrany M S and Al-Azmi A 2016 Potential applications of cold sprayed Cu50Ti20Ni30 metallic glassy alloy powders for antibacterial protective coating in medical and food sectors *J. Mech. Behav. Biomed. Mater.* **56** 183–94
[190] Silveyra J M, Ferrara E, Huber D L and Monson T C 2018 Soft magnetic materials for a sustainable and electrified world *Science* **263** eaao019
[191] Gutfleisch O, Willard M A, Brück E, Chen C H, Sankar S G and Liu J P 2011 Magnetic materials and devices for the 21st century: stronger, lighter, and more energy efficient *Adv. Mater.* **23** 821–42
[192] Azuma D and Hasegawa R 2008 Audible noise from amorphous metal and silicon steel-based transformer core *IEEE Trans. Magn.* **44** 4104–6
[193] Wang A, Zhao C, Men H, He A, Chang C, Wang X and Li R-W 2015 Fe-based amorphous alloys for wide ribbon production with high Bs and outstanding amorphous forming ability *J. Alloys Compd.* **630** 209–13
[194] Wang A, Zhao C, He A, Men H, Chang C and Wang X 2016 Composition design of high Bs Fe-based amorphous alloys with good amorphous-forming ability *J. Alloys Compd.* **656** 729–34
[195] Ogawa Y, Naoe M, Yoshizawa Y and Hasegawa R 2006 Magnetic properties of high Bs Fe-based amorphous material *J. Magn. Magn. Mater.* **304** e675–e7
[196] Shi L and Yao K 2020 Composition design for Fe-based soft magnetic amorphous and nanocrystalline alloys with high Fe content *Mater. Des.* **189** 108511
[197] Li H, Wang A, Liu T, Chen P, He A, Li Q, Luan J and Liu C-T 2021 Design of Fe-based nanocrystalline alloys with superior magnetization and manufacturability *Mater. Today* **42** 49–56
[198] Chen P, Wang A, Zhao C, He A, Wang G, Chang C, Wang X and Liu C-T 2017 Development of soft magnetic amorphous alloys with distinctly high Fe content *Sci. China Phys. Mech. Astron.* **60** 106111
[199] Chen P, Liu T, Kong F, Wang A, Yu C, Wang G, Chang C and Wang X 2018 Ferromagnetic element microalloying and clustering effects in high Bs Fe-based amorphous alloys *J. Mater. Sci. Technol.* **34** 793–8
[200] Zhao C, Wang A, He A, Chang C and Liu C-T 2021 Nano-heterogeneity-stabilized and magnetic-interaction-modulated metallic glasses *Sci. China Mater.* **64** 1813–9
[201] Zhao C, Wang A, He A, Yue S, Chang C, Wang X and Li R-W 2016 Correlation between soft-magnetic properties and Tx1-Tc in high Bs FeCoSiBPC amorphous alloys *J. Alloys Compd.* **659** 193–7
[202] Rohr L, Reimann P, Richmond T and Güntherodt H-J 1991 Refractory metallic glasses *Mater. Sci. Eng.* A **133** 715–7
[203] Yoshimoto R, Nogi Y, Tamura R and Takeuchi S 2007 Fabrication of refractory metal based metallic glasses *Mater. Sci. Eng.* A **449** 260–3
[204] Howard J, Carlson K and Chidambaram D 2021 High-temperature metallic glasses: status, needs, and opportunities *Phys. Rev. Mater.* **5** 40301
[205] Phillips W and Chidambaram D 2019 Corrosion of stainless steel 316L in molten LiCl-Li2O-Li *J. Nucl. Mater.* **517** 241–53
[206] Rodriguez D, Merwin A and Chidambaram D 2014 On the oxidation of stainless steel alloy 304 in subcritical and supercritical water *J. Nucl. Mater.* **452** 440–5
[207] Wang Y-T, He Q-F, Wang Z-J, Li M-X, Liu Y-H, Yang Y, Sun B-A and Wang W-H 2021 Exceptionally shear-stable and ultra-strong Ir-Ni-Ta high-temperature metallic glasses at micro/nano scales *Sci. China Mater.* **64** 1–7
[208] Wang Z, Li M, Yu J, Ge X, Liu Y and Wang W 2020 Low-iridium-content IrNiTa metallic glass films as intrinsically active catalysts for hydrogen evolution reaction *Adv. Mater.* **32** 1906384
[209] Carmo M, Sekol R C, Ding S, Kumar G, Schroers J and Taylor A D 2011 Bulk metallic glass nanowire architecture for electrochemical applications *ACS Nano* **5** 2979–83
[210] Chen J K, Chen W T, Cheng C C, Yu C C and Chu J P 2018 Metallic glass nanotube arrays: preparation and surface characterizations *Mater. Today* **21** 178–85
[211] Van Toan N, Tuoi T T K, Tsai Y C, Lin Y C and Ono T 2020 Micro-fabricated presure sensor using 50 nm-thick of Pd-based metallic glass freestanding membrane *Sci. Rep.* **10** 1–9
[212] Lin Y C, Tsai Y C, Ono T, Liu P, Esashi M, Gessner T and Chen M 2015 Metallic glass as a mechanical material for microscanners *Adv. Funct. Mater.* **25** 5677–82
[213] Kumar G, Desai A and Schroers J 2011 Bulk metallic glass: the smaller the better *Adv. Mater.* **23** 461–76
[214] Cai C N, Zhang C, Sun Y S, Huang H H, Yang C and Liu L 2017 ZrCuFeAlAg thin film metallic glass for potential dental applications *Intermetallics* **86** 80–7
[215] Li J, Doubek G, McMillon-Brown L and Taylor A D 2019 Recent advances in metallic glass nanostructures: synthesis strategies and electrocatalytic applications *Adv. Mater.* **31** 1–28
[216] Jang D and Greer J R 2010 Transition from a strong-yet-brittle to astronger-and-ductile state by size reductionofmetallicglasses *Nat. Mater.* **9** 215–9
[217] Li F C, Wang S, He Q F, Zhang H, Sun B A, Lu Y and Yang Y 2017 The stochastic transition from size dependent to size independent yield strength in metallic glasses *J. Mech. Phys. Solids* **109** 200–16
[218] Korkmaz S and Kariper A 2020 Glass formation, production and superior properties of Zr-based thin film metallic glasses (TFMGs): a status review *J. Non-Cryst. Solids* **527** 119753
[219] Chiang P T, Chen G J, Jian S R, Shih Y H, Jang J S C and Lai C H 2010 Surface antimicrobial effects of Zr61Al7.5Ni10Cu17.5Si4 thin film metallic glasses on Escherichia coli, Staphylococcus aureus, Pseudomonas aeruginosa, Acinetobacter baumannii and Candida albicans *Fooyin J. Health Sci.* **2** 12–20
[220] Jia H, Liu F, An Z, Li W, Wang G, Chu J P, Jang J S C, Gao Y and Liaw P K 2014 Thin-film metallic glasses for substrate fatigue-property improvements *Thin Solid Films* **561** 2–27
[221] Chu J P, Diyatmika W, Tseng Y J, Liu Y K, Liao W C, Chang S H, Chen M J, Lee J W and Jang J S C 2019 Coating cutting blades with thin-film metallic glass to enhance sharpness *Sci. Rep.* **9** 1–11
[222] Chu J P, Yu C C, Tanatsugu Y, Yasuzawa M and Shen Y L 2016 Non-stick syringe needles: beneficial effects of thin film metallic glass coating *Sci. Rep.* **6** 1–7
[223] Chu J P, Liao W C, Yiu P, Chiou M T and Su K H 2020 Metallic glass coating for improved needle tattooing performance in reducing trauma: analysis on porcine and pig skins *Sci. Rep.* **10** 1–12